2009

Radiative Transfer Models of the Galactic Center

Everett A. Schlawin
Oberlin College

Radiative Transfer Models of the Galactic Center
Senior Honors Thesis
Oberlin College Department of Physics and Astronomy

Everett Schlawin
Everett.Schlawin@gmail.com

April 1, 2009

Executive Summary

This thesis discusses research being done to understand the inner parts of the Milky Way Galaxy. We already know that there are dense star clouds, a supermassive black hole, and a large bar structure, but much of the inner galaxy is shrouded in mystery. Dust absorption, for one thing, prevents us from seeing the galactic center directly with our eyes.

To help understand the elusive inner Milky Way, we examine radio telescope data taken in Antarctica by Oberlin College Professor Chris Martin. His gigahertz radio observations were already analyzed to help understand how gas funnels into the Milky Way's supermassive black hole. We study this data further to characterize turbulence and predict how hot or cold the gas is.

The analysis of this data will also help prepare for the next thing: Herschel Space Observatory. This European telescope is scheduled to be launched in late April and will begin taking data in the fall of 2009. Chris Martin was granted 125 hours of observation time on the telescope to study the Inner Milky Way.

Acknowledgements

Professor Chris Martin has been an invaluable resource for this project. I have been very fortunate for his computer expertise, astronomical knowledge, and jovial enthusiasm throughout my project. There are few advisers so capable and willing as he to make their undergraduates' experience a perfect one. Additional thanks to the full Antarctic Submillimeter Telescope and Radio Observatory (AST/RO) team for their data.

Graduate students Ryan Porter and Eric Pellegrini gave me important tips on Cloudy and how to get the models to best match the clumps. In particular, Eric suggested I investigate the sources of heating for our clouds and whether to include turbulence in the models. Their help was especially kind, considering that they had no incentive to help me but the betterment of science. Sophia Chen has helped me see the bigger picture and put this project in the context of astronomy. Her questions and feedback on this paper were important checks on its legibility and helped me target it towards the general physics audience.

Adam Ginsberg's advice was a useful for making qualitative and analytical calculations to help check on Cloudy. I appreciate his willingness to help and for hosting me in Colorado while I visited the school and talked to him about the Interstellar Medium. I should also thank John Bally for writing up notes about optical depth which Adam Ginsberg forwarded to me.

Thanks to my family and Julie for putting up with my time needs on this project. They have been very understanding of my commitments and have encouraged me throughout the process. Extra thanks for Julie for helping edit my work. Her enthusiasm and good spirits got me through the final stretch on this project. At the last minute, she provided a wealth of great comments and suggestions to my thesis and provided me with the energy necessary to get to the last final stretch. Brian Burkholder also helped edit and evaluate my physics. I appreciate his help even when he was burdened with his own thesis to work on.

Table of Contents

List of Figures

Chapter 1

Introduction

Figure 1.1 The Milky Way is visible to the naked eye away from bright city lights. As evident in this photograph from Hepburn (2008), the central bulge is close to the constellation Sagittarius. A dark band of dust along the plane of the Milky Way blocks our view of the stars behind it.

1.1 The Milky Way

On a clear dark night, away from city lights, the sky is awash with stars and the glow of the Milky Way. The vast majority of what we see is part of the Galaxy[1] itself. Only a few other galaxies like Andromeda emit enough light to be seen from Earth with the naked eye.

We are surrounded in all directions by Milky Way stars because we are deep in the Galactic disk. If our vantage point were farther away, we might have some idea of what the Galaxy looks like as a whole, but we are left to mathematical techniques to actually map out the big picture. Even with today's telescopes and computers, the actual shape of the Galaxy is still uncertain.

[1]When Galaxy is capitalized, it means the Milky Way Galaxy to astronomers.

One problem is illustrated by Figure 1.1, where there is a dearth of stars seen along the plane of the Galaxy. This is where we should see the thickest concentration of stars, but instead we see dark lanes! The culprit here is dust extinction; light from the Galactic Center, for example, is diminished by a factor of 10^{12} (Law, 2007). This is because micron-sized dust particles absorb sub-micron wavelength light very efficiently. As explained in the Mie Theory (Carroll & Ostlie, 2006), dust absorption is like water wave absorption by rocks in a lake. Fist-sized rocks will do little to slow down wide swells, but may be effective blockers of ripples that have a wavelength close to the size of the pebble.

The other difficulty when observing the Milky Way "source confusion"—nearby gas looks a lot like distant gas so it is hard to figure out which is which. There are ways to get around source confusion (from velocity measurements) and ways to see through dust (from longer-wavelength observations), but they still do not give a clear unambiguous picture of our Galaxy. In a sense the Galaxy is still a jigsaw puzzle, where we can see most of the pieces but not position them in the right place. This paper describes some of the work being done to understand the Inner Galaxy, where astronomers are working on the middle piece in the Galactic Jigsaw Puzzle.

1.2 The Galactic Center

If we could travel into the very center of the Milky Way, we would find newly born stars, bright gas clouds and high densities ($n_{H_2} \gtrsim 10^4$ cm^{-3}). For reference, the Earth's atmosphere has $n_{N_2} \approx 10^{19}$ cm^{-3} so "high density" gas is a relative term. This region is called the Galactic Center, or GC, though different astronomers use different sizes when describing it. 400pc will be adopted as the GC radius for this text.[2] It consists of a number of H II regions,[3] molecular clouds, radio filaments, supernova remnants (SNRs), star clusters and a super-massive black hole. Due to the intervening gas and dust, this region of the Milky Way is invisible to optical detectors. Astronomers must use radio, infrared, and X-Ray telescopes to explore this region of the Milky Way.

The GC is a major stellar birthplace. The most active star formation occurs in a ring between radii of 70 and 175pc surrounding the center of the GC (Law, 2007). Young star clusters created in this ring tend to migrate inwards as they lose energy. Such clusters, like the Arches, Quintuplet and Central star clusters power and light up gaseous features like the Arched Filaments, Sickle nebula and Sgr A complex. Other prominent features include SNRs, which are corpses of large stars that underwent supernovae and spewed out shells of gas (Law, 2007).

1.3 The Inner Galaxy

Stepping back from the GC a little bit, we are in the realm of the Galactic Bar. This region, roughly 1 kpc (kilo-parsec) in radius surrounding the GC is the Inner Galaxy (IG). Here, the dynamics of gas are controlled strongly by the Bar (Häfner et al., 2000). The Bar's gravitational potential creates bizarre orbital curves that look nothing like the Earth-Sun system's elliptical-orbit. The IG orbits instead have cusps, asymmetries, irregularities and self-intersections. Only two families of curves, dubbed $x1$ and $x2$, have non-intersecting orbits. These are important curves for orbiting gas because self-intersections are unstable; extended gas structures that collide with themselves will tend to lose orbital angular momentum through shocks and move to a new orbit. The $x1$ family is a set of cusped orbits more than 500pc from the center of the Galaxy, while the $x2$ orbits are within 400pc. In between, at a radius of roughly 450pc, is the Inner Lindblad Resonance (ILR). The ILR is the distance at which the epicyclic frequency (the frequency of deviations from elliptical orbit) equals the pattern speed of the bar (the speed of a rigidly rotating bar). The Galactic Bar tends to pull gas towards the ILR, where it accumulates in a ring 900pc in diameter (Stark et al., 2004).

[2] 1 parsec (pc) is 3.26 light years or 3.09 $\times 10^{16}$ m.

[3] H II regions are where hydrogen is singly-ionized - the Roman numeral I indicates neutral H emission and II indicates emission from H^+ ions

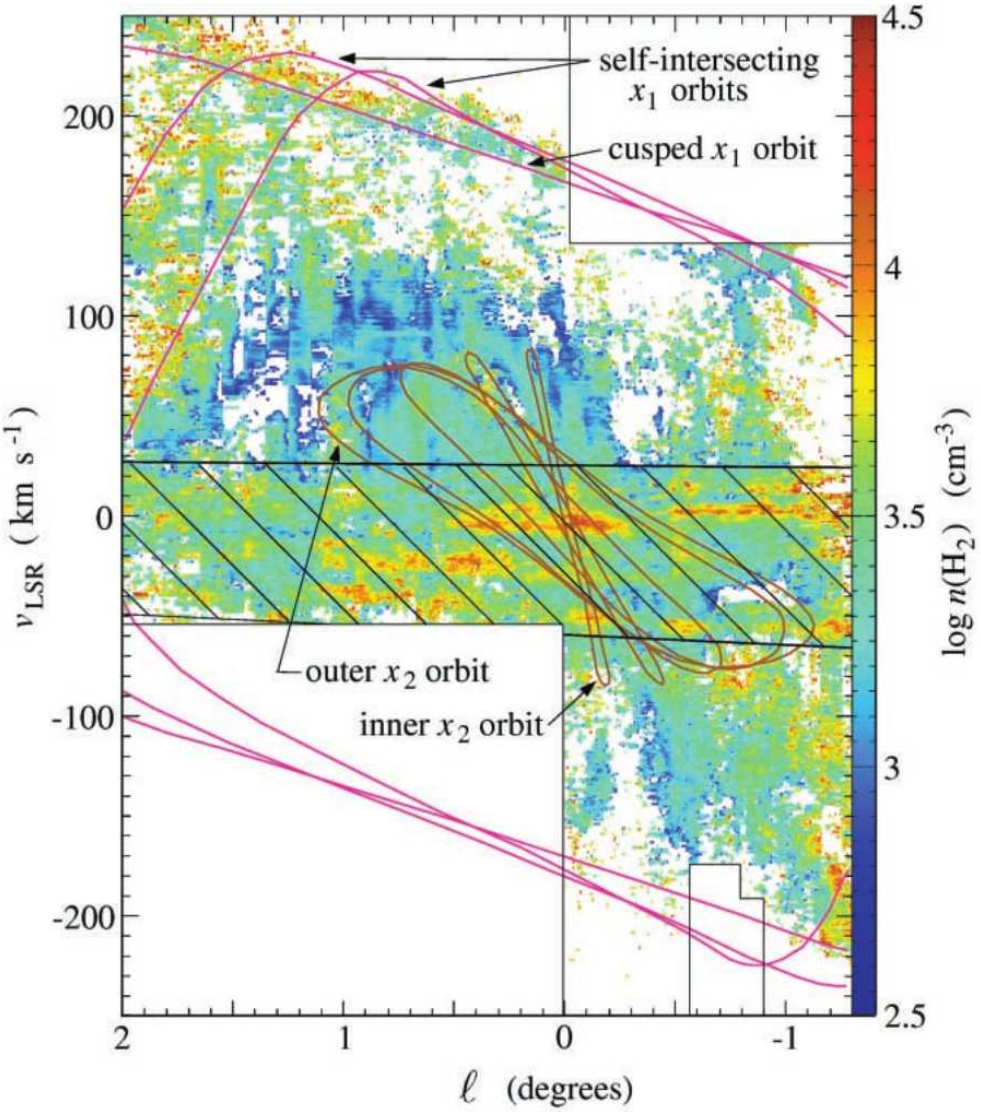

Figure 1.2 Schematic of Inner Galaxy orbits from Stark et al. (2004). $x1$ and $x2$ orbits are of key concern because they contain non-intersecting curves on which gas may orbit relatively stably. As found by Stark et al. (2004), gas tends to be drawn towards the Inner Lindblad Resonance (ILR) located between the $x1$ and $x2$ curves.

As gas accumulates and the density increases, it approaches the point of gravitational collapse. This occurs when the self gravity of a clump exceeds the tidal forces (from the Galactic Center and Bar) tearing it apart. As found by Stark et al. (2004), the density of molecular hydrogen needed for collapse is $n(H_2) > 10^{3.5}$ cm^{-3} $(\kappa/ 10^{12}\mathrm{yr}^{-1})^2$ where κ is the epicyclic frequency of a cloud. After this threshold is reached and a cloud collapses, it experiences dynamical friction with the surrounding stars and falls toward the Galactic Center. Dynamical friction is a force caused by the accretion of material behind a compact cloud or star moving through a medium of other stars and gas. The compact moving object pulls parts of its medium towards it and then a slight over-density develops behind the object in question. This will happen continuously for a moving object until the gravitational tug caused by the over-densities behind slows down the compact moving object. For the Inner Galaxy, this slowing-down sends the star or compact cloud

on a downward spiral towards the Milky Way's supermassive black hole. Thus, the ILR empties out and the process begins again, much like the voltage in an RC oscillator. The period of this cycle is believed to be 20 million years.

1.4 Cloud Morphology

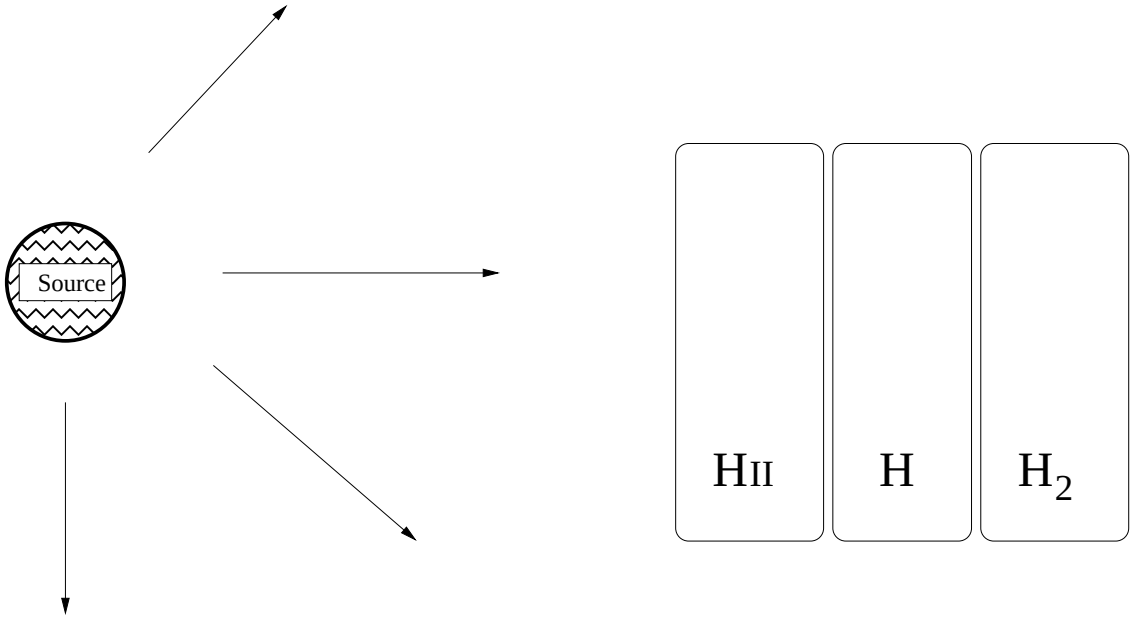

Figure 1.3 Schematic of a plane parallel model of a cloud. The star on the left will heat up the gas nearest to it and ionize the hydrogen. This is called the H II region. Farther out, where the photon flux is weaker, there is atomic hydrogen. The photons still have enough energy ($\approx$ 6eV to 13.6eV) to keep hydrogen molecules from forming. Only when these ultraviolet photons are extinguished does molecular hydrogen form. This happens in the most dense regions, farther still from the hot star, drawn in the right as H_2. More complicated geometries usually occur than the plane-parallel picture above, with bubbles shells or other curved surfaces.

The Interstellar Medium (ISM) is characterized by three regions: H II close to the sources of UV radiation, atomic H a little farther out, and molecular H_2 farther still. H II means there is radiation from singly-ionized hydrogen (H^+), so this gas is called an "H two"—H II region. It is also called the "ionized" region because the $\geq 13.6eV$ photons in this region strip electrons from the hydrogen atoms, creating H^+ from H^0. The atomic hydrogen region begins where these ionizing photons have become extinguished and ends where photons are so weak they cannot even break apart H_2 molecules. At this point, the gas is cold, dense, and black, and consists mostly of molecular hydrogen (H_2). Figure 1.3 shows these three regions in a "plane-parallel" model, where each shell of gas is approximately flat. This works well in many situations, such as the Earth's atmosphere, where the curvature is so slight that the air can be approximated as a flat layer parallel with the ground.

The plane-parallel model applies well over small angular scales, but this does not mean clouds are flat! They are often lumpy, curvy, bubbly or clumpy. In many cases, there is a shell of ionized gas (H II) enclosing a star and surrounded by a shell of molecular hydrogen. In other cases, there is a dense clump of molecular hydrogen (H_2) surrounded by atomic H. The clouds studied in this text are probably cases of the latter.

1.5 Molecular Clumps

Two interesting clumps were discovered by Bania (1977). His survey of the rotational CO $J = 1 \rightarrow 0$ transition in the IG revealed two isolated features standing out from the nuclear disk. Clump 1, at $\ell = 355^\circ$ and radial velocity $+100$ km s^{-1}, is noteworthy because its velocity and position forbid circular motion. Clump 2 stood out because of its very extended (50-150 km s^{-1}) velocity structure.

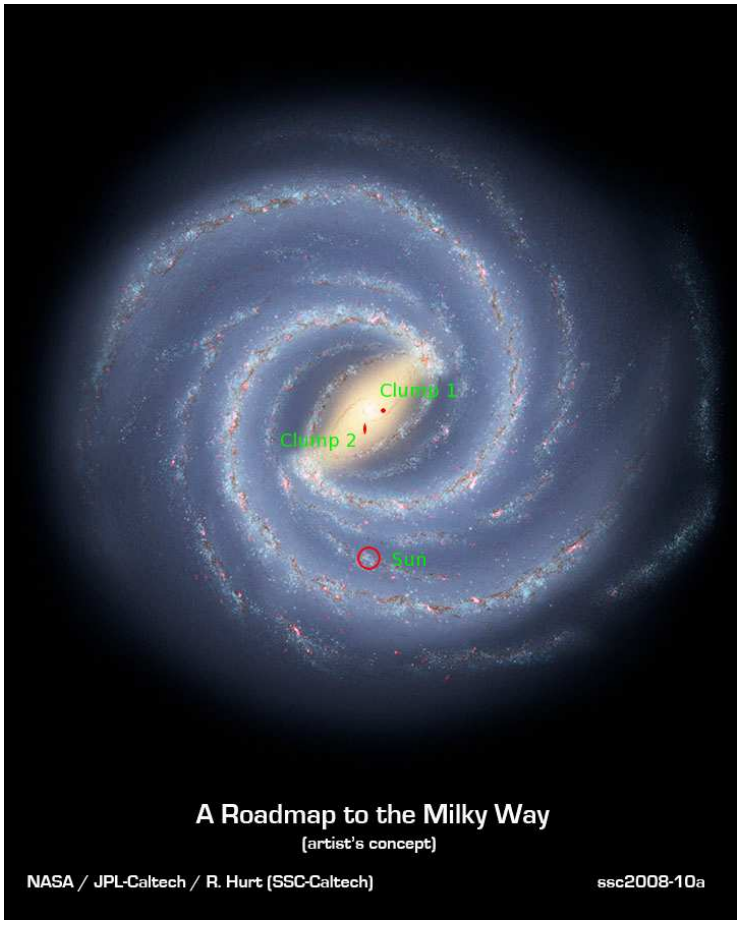

Figure 1.4 One possible projection of Clump 1 and Clump 2. Sawada et al. (2004) used a technique of measuring foreground absorption against Galactic Center continuum emission. See §1.5.3 and Figure 1.8 for their method and predictions.

Figure 1.4 shows approximately where these two gas clumps lie in the Milky Way. For reference, Figure 1.5 shows the Galactic Coordinate system. The plane of the galaxy lies along $b = 0^\circ$.

1.5.1 Clump 1

Clump 1 is a typical molecular cloud with an atypical velocity ($\ell \approx 355^\circ$, $b \approx +0.4^\circ$, $v_{\rm LSR} \approx +100$ km s^{-1}). Such high positive velocity in the IG indicates that it has the largest non-circular orbit in the Galaxy. At a minimum, Clump 1 is ∼1 kpc from the GC, but it may be more like 3 kpc distant, depending on which dynamical model and which distance-marker one uses. The 3kpc estimate associates Clump 1 with a $+135$ km s^{-1} arm extending from a central molecular ring. Bania et al. (1986) predict that the cloud dimensions are 42 pc × 72 pc and predict it to

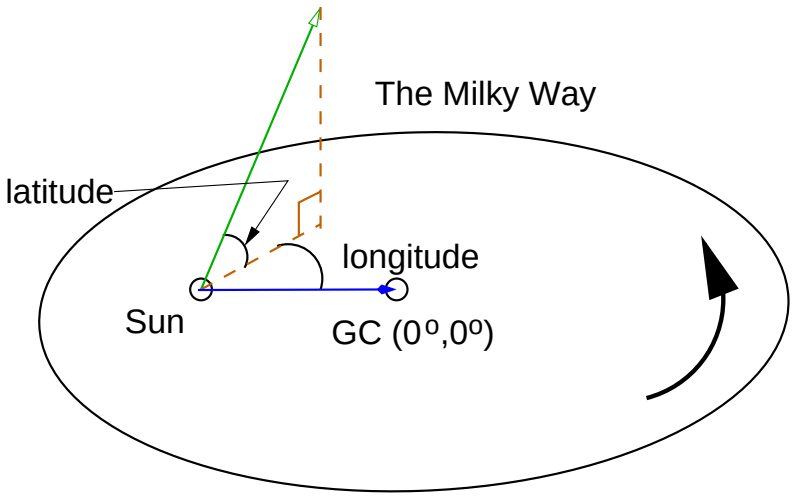

Figure 1.5 Galactic longitude ℓ and latitude b are shown in the figure. These are the angles measured from the Galactic center so that the GC is (ℓ=0°,b=0°). This figure is copied from the one in Carroll & Ostlie (2006).

have a total mass $\approx 2.4 \times 10^5\ M_\odot$.[4] According to their models, the majority of the gas is in molecular hydrogen (H_2) form, with atomic hydrogen (H) making up $\leq 10\%$ of the clump. This mass estimate was a revision from an earlier prediction of $9 \times 10^6\ M_\odot$ (Bania, 1977).

Bania et al. (1986) show that Clump 1 is actually a part of a complex of three different clumps including itself, Clump 3 and Clump 4. These, in turn, are made of even smaller pieces. Together, they are not too dissimilar from groups of Giant Molecular Clouds found in other parts of the Galaxy. Clumps 3 and 4 are in the same line of sight as Clump 1, but they have slightly different velocities, $+85\ \mathrm{km\,s^{-1}}$ and $+68\ \mathrm{km\,s^{-1}}$, respectively. According to Bania et al. (1986), the excitation temperature, $T_{ex} \approx 10$ K. Excitation temperature will be discussed in §2.1.

Clump 1 is different from 3 and 4 in that it has an associated H II region, G354.67+0.25. This ionized region probably contains a few hot stars that radiate energy and thus add heat to Clump 1, even though G354.67+0.25 has a weak energy output and small mass $M_{HII} \approx 7 \times 10^3\ M_\odot$. It is possible that G354.67+0.25 is ionized entirely by a single O5 or O6 star—this kind of star has a surface temperature larger than 30,000K (Carroll & Ostlie, 2006). Whether it is one star or three, such a small energy output is unlikely to have kicked Clump 1 into its large non-circular orbit. The low power of G354.67+0.25 also eliminates the possibility that Clumps 3 and 4 are blasted-off parts of Clump 1. Instead, gravitational effects in the Inner Galaxy are the most likely causes for the clumps' positions and velocities (Bania et al., 1986).

The Antarctic Submillimeter Telescope and Radio Observatory (AST/RO) made more recent observations of Clump 1, measuring the ^{13}CO $J = 2 \rightarrow 1$, CO $J = 7 \rightarrow 6$, CO $J = 4 \rightarrow 3$, and [C I] $^3P_1 \rightarrow {}^3P_0$ emission (Martin et al., 2009). The results are seen in Figure 1.6, where the intensity peaks at ℓ=-5.15°and b=0.4°. The one exception is CO $J = 7 \rightarrow 6$, which is virtually nonexistent, probably because the gas is not warm enough to excite CO to the $J = 7$ state.

1.5.2 Clump 2

Clump 2 ($\ell \approx 3°$, $b = 0.2°$, v=-20 to 150 $\mathrm{km\,s^{-1}}$) has the largest velocity width of any known Galactic CO structure (See Figure 2.3 for a description of line width). While a typical GMC has a velocity width of 5 km/s, Clump 2 appears to have a width of 170 km/s. A possible explanation is that it is made of several smaller clouds. Indeed, high spectral resolution measurements reveal

[4] $M_\odot$ stands for solar mass, 1 $M_\odot$= 1.99 $\times 10^{30}$ kg

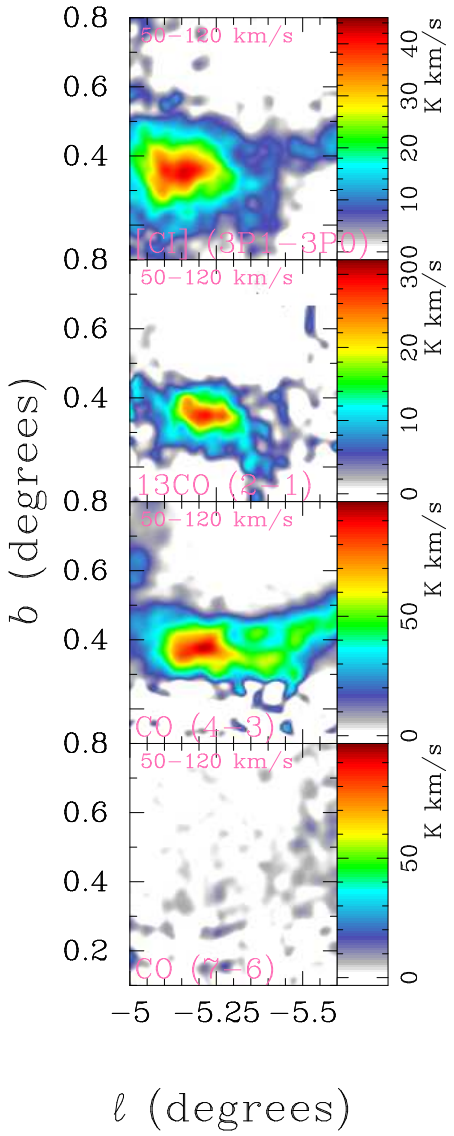

Figure 1.6 Clump 1 ^{13}CO $J = 2 \rightarrow 1$, CO $J = 7 \rightarrow 6$, CO $J = 4 \rightarrow 3$, and [C I] $^3P_1 \rightarrow {}^3P_0$ emission, from Antarctic Submillimeter Telescope and Radio Observatory (Martin et al., 2009)

that there may be as many as 16 components along $\ell = 3°$. These individual components have more typical GMC widths. Their velocity structure is explicable with simple circular motion, indicating that the center-most cloud is 470 pc from the GC (Stark & Bania, 1986).

The H_2 densities and masses for the cores within Clump 2 would ordinarily indicate ongoing star formation. However, the 8 μm features usually present in star forming regions are absent from the Galactic Legacy Infrared Mid-Plane Survey Extraordinaire (GLIMPSE) 8 μm image. There is one small (arcminute size) bubble seen in the GLIMPSE data, possibly associated with IRAS 17470-2533, but the rest of the region has essentially no signatures of star formation (Bally et al., 2009).

Clump 2 has very weak to no HNCO (isocyanic acid) emission. HNCO emission generally requires H_2 densities $\geq 10^6$ cm^{-3}, so it is considered a tracer of very dense gas. HNCO also traces very strong Far-Infrared emission, so Clump 2 probably has no extreme over-densities or super-strong FIR emission (Dahmen et al., 1997).

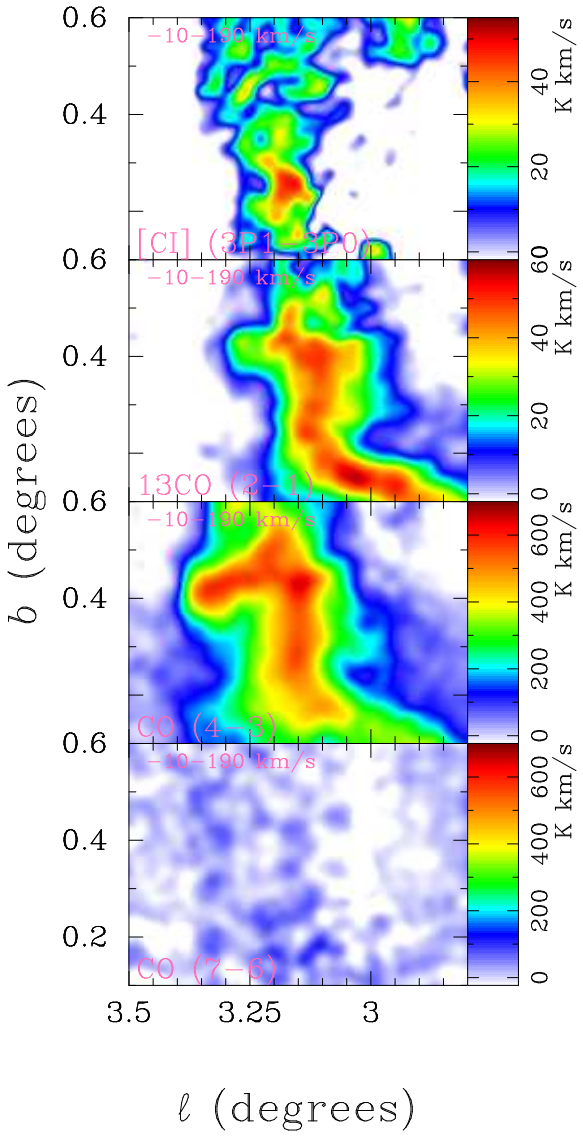

Figure 1.7 Clump 2 ^{13}CO $J = 2 \rightarrow 1$, CO $J = 7 \rightarrow 6$, CO $J = 4 \rightarrow 3$, and [C I] $^3P_1 \rightarrow {}^3P_0$ emission, from Antarctic Submillimeter Telescope and Radio Observatory (Martin et al., 2009)

1.5.3 Spatial Mapping

One way to measure distance is by analyzing cloud spectra. The advantage of this method is that it does not require any assumptions about the orbital mechanics of the Inner Galaxy. Sawada et al. (2004) use absorption of OH and emission of CO to infer distance relative to the Galactic Center continuum source. The principle of their technique is that gas in front of the continuum absorbs light, while gas behind the source cannot. The method works well for mass along the line of sight to the central continuum, but not so well to the sides.

As Sawada et al. (2004) show, the ratio of OH absorption to CO emission indicates distance. They use CO as a proxy for gas density as it passes through most of the Interstellar Medium. 1667 MHz OH, on the other hand gets absorbed. The ratio of these two lines gives an indication of distance; with OH/CO close to 0, one predicts gas to be behind the continuum source and larger ratios indicate gas in front.

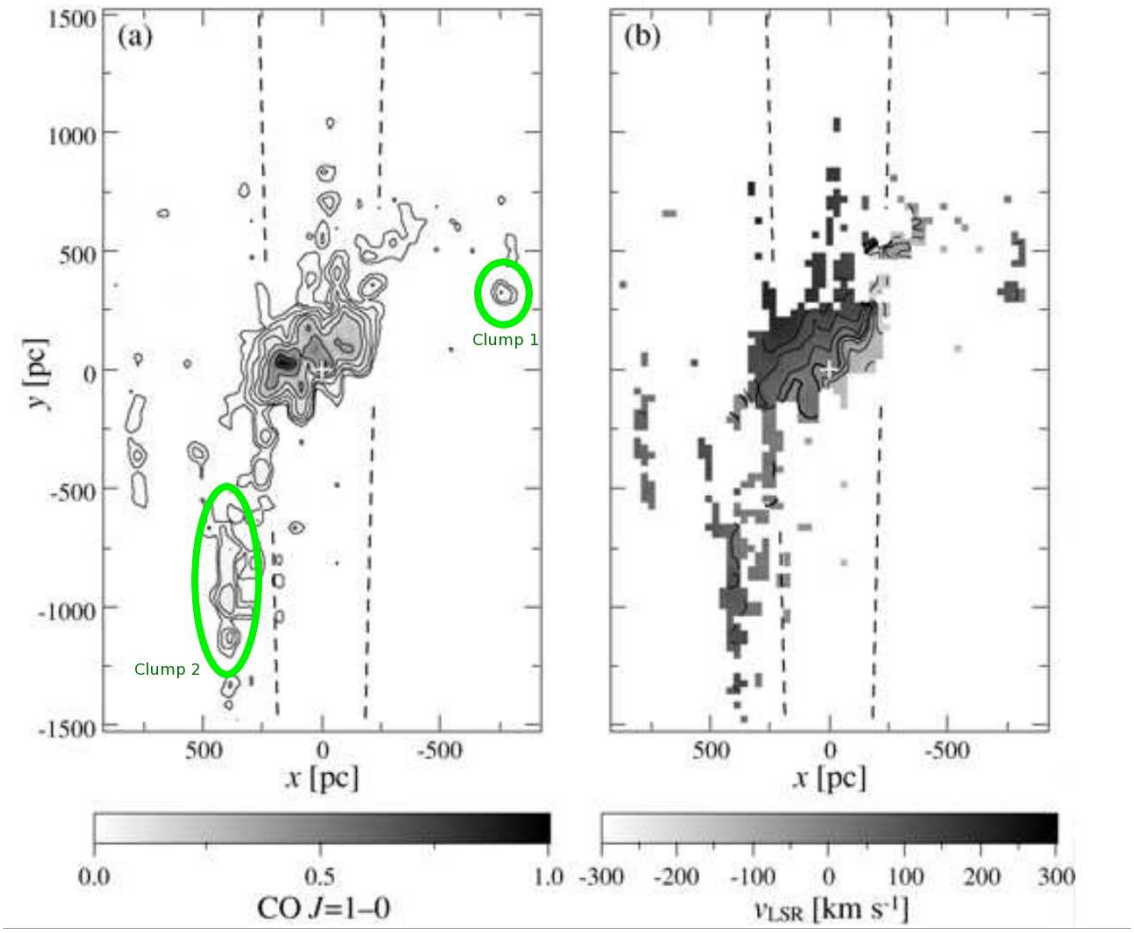

Figure 1.8 Face-On View of The Galactic Center, from Sawada et al. (2004)

Sawada et al. (2004) take two-dimensional spectra in longitude-velocity space and map out a bird's-eye view of the structure. They predict Clump 1 to be roughly 70 pc in diameter and Clump 2 to be an oblong structure, 700 pc wide by 500 pc deep along the line of sight. Clump 2 is predicted to lie 800 pc in front of the GC and its smaller companion is predicted to be behind. The Clump 1 predictions are less trustworthy as their spectral mapping method works only for gas along the line of sight to the continuum source.

1.6 Herschel Space Observatory

There are still many unanswered questioned about Clump 1 and Clump 2. How accurate are the 1986 mass predictions? What are their main sources of heating? When will they spiral into the Galactic Center's black hole? Are they pieces of the Milky Way that continually fall into the GC or remnants of some other galaxy?

The answer to these questions may come from the Herschel Space Observatory. Herschel will observe the far infrared and sub-millimeter sky (55 to 672 microns) with sensitivity far exceeding that of any previous mission. Its 3.5 meter mirror will focus light onto one of three instruments. The two imagers and medium-resolution spectrometers (Photodetector Array Camera and Spectrometer (PACS) and Spectral and Photometric Imaging Receiver (SPIRE)) are complemented with a very high resolution spectrometer Heterodyne Instrument for the Far Infrared (HIFI). It will sit at the second Lagrange point, L2, essentially on the far side of the Earth from

the Sun. The telescope must be kept extremely cold with liquid helium and thus is projected to last as long as the coolant does—three to four years (Pilbratt, 2008). Its main observing goals are to help trace the birth and evolution of both galaxies and stars. Chris Martin, Principal Investigator for the Herschel Inner Galaxy Gas Survey (HIGGS) project, was granted 125 hours of observation time on Herschel to study Clump 1 and Clump 2.

Figure 1.9 Herschel Observatory after completion of some mechanical tests for stability (ESA, 2009).

1.6.1 Emission Lines of Interest

Herschel will have the capability to observe some infrared emission lines never seen before in these clumps. It will observe these with very high spectral resolution (good wavelength measurements) and the same spatial resolution (the smallest resolvable angular size) as AST/RO. These will include the five lines in Table 1.1.

The brightest line is likely to be [C II] at 158 μm. This is an important coolant for cold neutral-Hydrogen gas all over the Milky Way and other galaxies—see §2.3. This bright line, however, may come from ionized hydrogen as well as neutral hydrogen. To help differentiate this emission from these spatially-distinct places, we can use the [N II] 205 μm line. The 205 μm line brightness is almost directly proportional to [C II] 158 μm line for *ionized* regions (Oberst et al., 2006), because both C^+ and N^+ have similar secondary ionization potentials at 24.4eV and 29.6eV, respectively. This means that the conversion of C^+ into C^{++} and N^+ into N^{++} occur under nearly the same conditions. At an electron temperature, T_e, of 8000K, the two lines also have very close critical densities of 46 $cm^{-3}$and 44 cm^{-3}, respectively. With these nearly identical properties for ionized regions, the [N II] to [C II] ratio is expected to be constant. The situation changes, however, for *neutral* hydrogen gas. For these regions, [N II] cannot exist because the ionization potential of Nitrogen is 14.53eV, compared to 13.6eV for hydrogen. Carbon, on the other hand, has an

ionization potential below 13.6eV and [C II] emission is very strong in neutral regions. Therefore, [N II] can be used to separate [C II] emission that originates from ionized versus neutral gas.

Line	λ (μm)	Ionization Potential (eV)	$\Delta E/k$ (K)
C I	370	N/A	39
[C II]	157.7	11.3	91
[N II]	205	14.5	70
[N II]	122	14.5	118
[O I]	63	N/A	229

Table 1.1 Lines to be observed by Herschel Space Observatory

Chapter 2

Theory

Theoretical astrophysics tries to answer basic questions about the interstellar medium: What is it like inside distant gas clouds? How heavy are they? How are they heated? Will they form stars? The answer to these questions requires physical calculations because the direct observational evidence is usually very scarce.

The gas clouds studied in this paper are thousands of light years away and completely inaccessible for direct measurement. Without this access, we are left to discover what we can with statistical mechanics. A full discussion of this subject with numerical models is beyond the scope of this paper, but the following two chapters describe some of the aspects of interstellar medium modeling.

2.1 Temperature

When someone says, "The water is 115 degrees Fahrenheit," it is pretty clear what they mean. A thermometer stuck in the water will read 115°F. The water is at thermodynamic equilibrium, meaning molecules have a Maxwell-Boltzmann velocity distribution. In space, however, the Maxwellian temperature is insufficient because molecules, ions, electrons, and dust in the interstellar medium are usually not in equilibrium. Instead, astronomers use several different temperatures to describe the conditions within a gas. We discuss them in the next section.

Kinetic Temperature, $\mathbf{T}_k$

When we say, "The temperature of a cloud is ...", we are usually talking about kinetic temperature. The kinetic temperature characterizes the Maxwell-Boltzmann velocity distribution (Carroll & Ostlie, 2006):

$$n_v dv = n \left(\frac{m}{2\pi k T_k} \right)^{3/2} e^{(-mv^2)/(2kT_k)} 4\pi v^2 dv \tag{2.1}$$

where $n_v dv$ is the number density of particles within a velocity range dv as a function of n—the overall number density, m—the average mass and v—the velocity of the particles. This is the most familiar definition of temperature for physicists, because it describes gas in thermodynamic equilibrium well.

Excitation Temperature, $\mathbf{T}_{ex}$

When two states are in thermal equilibrium, the relative population of the states, n_1 and n_2 is found by the Boltzmann distribution:

$$\frac{n_2}{n_1} = \frac{g_2}{g_1} e^{(E_2 - E_1)/(kT_{ex})} \tag{2.2}$$

where g_1 and g_2 are the degeneracies of states 1 and 2. The above equation also defines T_{ex} for non-equilibrium cases. For example, suppose $n_2/n_1 = e^{-2}$ and $\Delta E/k = 92$K. Equation 2.2 says that T_{ex} is 46K, but the gas's kinetic temperature,T_k, could be 120K. In this case, T_{ex} simply indicates the relative population densities between n_2 and n_1, but these two species could be way out of whack with the rest of the system. T_{ex}, therefore, is only relevant for comparing two populations and will not necessarily describe the system's overall temperature.

Rotational Temperature, T_{rot}

Rotational temperature is almost identical to T_{ex}, except that it specifically refers to rotational transitions. In other words, n_1 and n_2 are the densities of two rotational states. Quantum mechanical selection rules say that only transitions with $\Delta J = \pm 1$ are allowed, so n_2 and n_1 are two states such that $J_1 = J_2 \pm 1$.[1]

Brightness Temperature, T_B

A perfect blackbody at a temperature T_B emits radiation with intensity given by (Carroll & Ostlie, 2006)

$$I_\nu = \frac{2h\nu^3}{c^2} \frac{1}{e^{(h\nu)/(kT_B)} - 1} \tag{2.3}$$

but real objects never have perfect blackbody spectra. Instead, they usually have emission peaks and absorption valleys on top of a blackbody curve, but this does not stop astronomers from using the blackbody formula anyway. At a given frequency, the only free parameter is temperature, so equation 2.3 provides an easy way to calculate intensity from that temperature. For logical reasons, the temperature associated with a particular intensity is called brightness temperature, T_B and it differs from T_k when the system strays from blackbody intensity.

Antenna Temperature, T_A*

When radio astronomers measure brightnesses, they often report the value as antenna temperature, T_A*. This is essentially the same as T_B, but may be smaller if a radio telescope detects a point source. In this case, T_A* measures the average T_B over the size of the telescope's spatial uncertainty, but T_B would represent the intensity directly along the line of sight of the point source. For extended sources, however, $T_A^* = T_B$ because in extended sources average brightness will be the same as its local brightness.

Electron Temperature, T_e

Electrons are not always in equilibrium with the atoms and molecules of a cloud. Therefore, T_e may be different from the rest of the cloud. The electron temperature is like the kinetic temperature, T_k except that the mass and velocity in the Boltzmann distribution become the mass and velocity of the electrons. T_e can easily differ from T_k when there is a magnetic field because electrons, with much smaller masses than protons, are more readily accelerated.

2.2 Heating

Heating is the process of adding energy to a system. If the system is a cloud of gas, heat is added primarily by photons, cosmic rays, supernovae shocks, compressional heating, and turbulence. For this paper, we consider photons, cosmic rays, and turbulence because shocks and compression are not thought to be present near Clump 1 and Clump 2. This is primarily because there is little evidence for star formation activity (see § 1.5.2), which is usually coincident with compression

[1]For the reader unfamiliar with rotational energy states for a rigid rotor, E = B J (J + 1) where B is the rotational constant and J=0,1,2,3,...

and supernovae. The heating sources we consider, through absorption and collisions, add kinetic energy to atoms, ions, and molecules in a gas.

2.2.1 Photons

The most important heating photons are usually ultraviolet photons, while soft X-Rays play a secondary role (Wolfire et al., 1995). Ultraviolet photons are absorbed largely by dust grains of 1nm to 30nm in size. In the process of absorption, they tend to eject electrons due to the photoelectric effect. The ejected electrons go on to add kinetic energy to the cloud. The total flux of the ultraviolet photons is very important for gas conditions, but the shape of the spectrum matters less (Wolfire et al., 1995). For this reason, the integrated flux of all photons between 6 eV and 13.6 eV is described in terms of the Habing field with the unit-less parameter G_o. When G_o= 1, the integrated flux is 1.3×10^{-4} erg $s^{-1}\,cm^{-3}$. In Clump 2, we expect G_o to be small because there is little evidence of hot stars in the area. Clump 1 may be heated by weak ultraviolet photons, so G_o should be slightly higher in this cloud.

2.2.2 Cosmic Rays

Cosmic rays are charged particles with high energies ($\gtrsim 10^9$ eV). One way to measure their importance is through the ionization rate, $\zeta_{\rm CR}$. From both diagnostic tools, like HCO^+ and CO emission and from direct measurements from the Voyager and pioneer spacecraft, $\zeta_{\rm CR} \approx 3 \times 10^{-17} s^{-1}$ in the solar neighborhood (van der Tak et al., 2006). In diffuse clouds toward the GC, $\zeta_{\rm CR}$ may be 10 to 100 times this rate and in dark clouds, $\zeta_{\rm CR}$ can drop to 1/10 the solar value. Oka et al. (2005) find that $\zeta_{\rm CR} \approx 10^{-15} s^{-1}$ in the GC while van der Tak et al. (2006) find $\zeta_{\rm CR} \approx 4 \times 10^{-16} s^{-1}$ in Sgr B. The cause of this variation is not entirely certain: it could be from variations in cosmic ray flux (as believed by van der Tak et al. (2006)) or from absorption and scattering of cosmic rays in these different objects. We expect stronger cosmic ray heating in the Inner Galaxy (IG) because there are more stars there and hence a greater number of ejected particles.

2.2.3 Turbulence

Turbulence can add heat to a cloud when the energy from large scale motions dissipates as thermal kinetic energy. This occurs in a cascade; the largest scale motions power intermediate size eddies, which in turn power smaller eddies. The energy cascades down to the smallest length scale, until it is turned into heat as illustrated in Figure 2.1.

The amount of dissipated energy from a turbulent cascade is usually not large enough to power an entire cloud (Lequeux, 2005). Ambient Galactic starlight in the solar neighborhood, for example, can add more energy to a cloud than the typical estimates for turbulent dissipation. One might then be tempted to discard turbulence as irrelevant; however, it is possible for turbulent eddies to concentrate energy in a local environment, significantly enhancing the amount of local heat dumped in a cloud. This phenomenon, called dissipative intermittency, is addressed further in §2.6. As an additional reason for studying turbulence, Clump 1 and Clump 2 are interacting strongly with the Galactic Bar and show the potential for very strong turbulent motions.

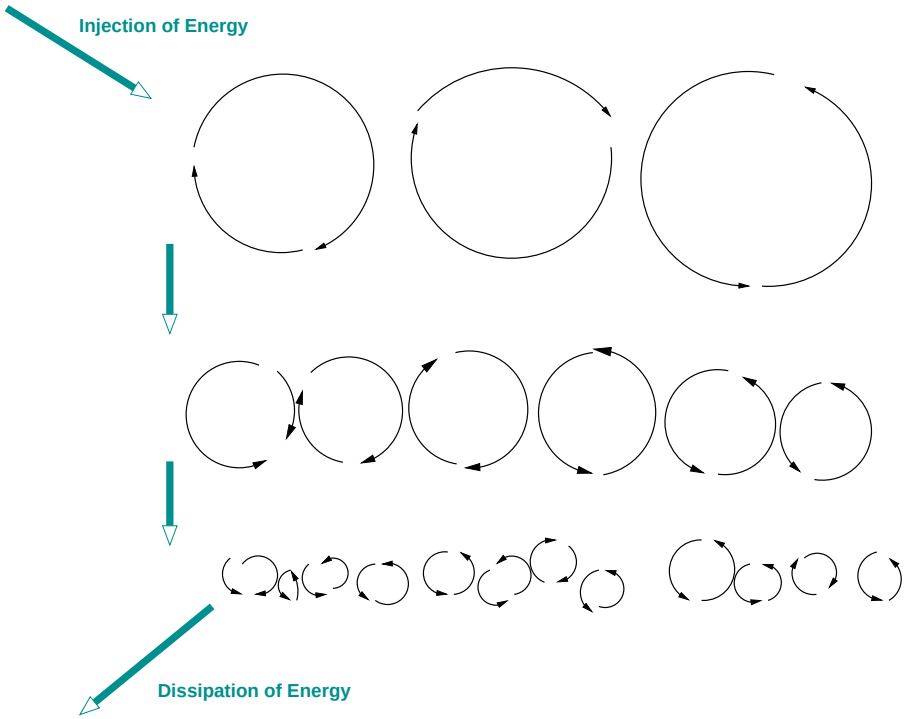

Figure 2.1 Large scale eddies tend to stir up smaller turbulent motions in a fluid. These will then stir up even smaller eddies. The process continues down a cascade, carrying energy from large scale sizes to small ones, until the energy is finally dissipated as heat. This figure is only a cartoon, and it disguises the fact that all these eddy sizes should occur at once. The smaller motions are embedded in the larger ones, but illustrating this would make it harder to show the energy cascade. This figure is largely copied from Frisch (1995).

2.3 Cooling

Now that we have discussed how to get a cloud hotter and hotter, we need to explain how it releases this energy and avoids getting to an infinite temperature! For interstellar clouds, this occurs via radiation only because conductive and convective cooling are too slow (Dyson & Williams, 1997).

Radiative cooling occurs when excited species (atoms, ions or molecules) enter a lower energy state and emit photons. In more technical terms, cooling occurs because stimulated and spontaneous emission carry energy away. The rate at which this occurs varies strongly between different cooling mechanisms. Furthermore, the relative importance of different cooling processes changes with cloud conditions like density and temperature. To theoretically determine which processes control most of a cloud's cooling, we look for species that have frequent collisions, $\Delta E \leq$ the thermal kinetic energy, and short lifetimes of excited states (Dyson & Williams, 1997). Alternatively, we can conclude which processes cool a cloud by observation. If a cloud has very bright CO $J = 1 \rightarrow 0$ 115 GHz emission, as in the case of Clump 1 and Clump 2, then CO rotational de-excitation must be a key cooling process.

2.3.1 Cooling by Atoms, Ions and Molecules

An example of a strong coolant for gas at 100K is the C II $^2P_{1/2} \rightarrow ^2P_{3/2}$ 158 μm line. C II $^2P_{1/2} \rightarrow ^2P_{3/2}$ has $\Delta E/k_B = 92$ K, so it will be easily excited by 100K gas. This characteristic energy is not a sufficient condition for excitation; cooling also depends on the excitation cross section of C^+. As it turns out, C^+ has a large cross section, so it is a good coolant. Other ions,

like Fe^+ and Si^+ are good coolants for warmer gas, like 10^3 K. Atomic hydrogen, H, kicks in at even higher temperatures (10^4K) because H atomic transitions require higher energies. For cooler gas, like at 20K, CO $J = 1 \rightarrow 0$ and other CO transitions become more important.

When a cooling line is emitted, it does not necessarily escape its host cloud. The radiation can be scattered by other species or can be absorbed by the same process that created it in the first place. Determining just how this occurs is the subject of §2.4. The output spectrum, once calculated by radiative transfer, gives a way to relate internal gas conditions like density and temperature to the observations made by telescopes. Therefore, from an observational astronomer's point of view, cooling is the most important process in a cloud.

2.4 The Transfer Equation

The propagation of electromagnetic radiation from its source and how much it is diminished or amplified is called radiative transfer. Radiation intensity is measured in terms of power per unit area per steradian per frequency; this is called specific intensity, I_ν because it is the intensity at a particular frequency. Its cgs units are erg cm^{-2} sr^{-1} Hz^{-1}. For this text, $I_\nu(0)$ stands for the initial intensity of light before it enters a cloud. The extent to which the intensity, I_ν is amplified or diminished is calculated by the transfer equation,

$$\frac{dI_\nu}{ds} = -K_\nu I_\nu + \epsilon_\nu \tag{2.4}$$

where s is the distance along a line of sight, K_ν is the absorption coefficient, and ϵ_ν comprises the emission and scattering. The positive absorption coefficient always weakens the light (hence the negative sign before $K_\nu I_\nu$), but the ϵ_ν term can either strengthen or weaken it, depending on the amount of emission versus scattering. The transfer equation can be expressed equivalently as

$$\frac{dI_\nu}{d\tau_\nu} = S_\nu - I_\nu \tag{2.5}$$

by making a change of variable $\tau_\nu \equiv \int K_\nu \, ds$. τ_ν is a dimensionless quantity called optical depth. The reason for this substitution and the value of optical depth will be made clear in the next equation. If S_ν is constant, the equation can be solved for I_ν

$$I_\nu = I_\nu(0)e^{-\tau} + S_\nu(1 - e^{-\tau}) \tag{2.6}$$

As seen in this solution, the optical depth, τ_ν indicates the opacity of an interstellar object. When $\tau_\nu \gg 1$, this means a source is entirely opaque and anything beyond it is invisible. Emission like this is called optically thick emission. Conversely, when $\tau_\nu \lesssim 1$, the emission is called optically thin, and the cloud or gas is transparent. Equation 2.6 also makes the S_ν term more illuminating. S_ν is called the source function. Intensity tends to approach the source function as it progresses through the cloud. Progression in this case, means increasing τ_ν. When τ_ν is much larger than 1, $I_\nu = S_\nu$.

For systems with blackbody emissivity, the source function approaches the Planck distribution, B_ν.

$$B_\nu(T) = \frac{2h\nu^3}{c^2} \frac{1}{e^{\frac{h\nu}{kT}} - 1} \tag{2.7}$$

This somewhat complicated equation can be simplified in the case that $h\nu \ll kT$. Since we are working at long wavelengths, this approximation is valid. Using the first order Taylor expansion of an exponential, the Planck distribution becomes the Raleigh-Jeans approximation:

$$B_\nu(T) \approx \frac{2kT\nu^2}{c^2} \tag{2.8}$$

2.5 Simple Analytical Tools

A full treatment of heating, cooling, radiative transfer, and turbulence can be overwhelming. It has taken the combined work of many theorists to create spectral synthesis codes to carry out all the calculations. Hence, the entire story will not be discussed in this paper. Instead we will describe some of the more simple analytical tools that can be used for order-of-magnitude estimates.

2.5.1 How to Weigh a Cloud

The following section gives a simplified method for determining the mass of a cloud (Dyson & Williams, 1997). This particular method assumes that some source of light, with intensity $I_\nu(0)$, is obscured by a uniform composition of obscuring material. A useful way of measuring the total absorption is the equivalent width, defined to be

$$W = \int \left(1 - \frac{I_\nu}{I_\nu(0)}\right) d\nu \tag{2.9}$$

where I_ν is the intensity of a line at any given point and $I_\nu(0)$ is the original, unobscured intensity. W is essentially the area of the curve representing the absorption line divided by $I_\nu(0)$.

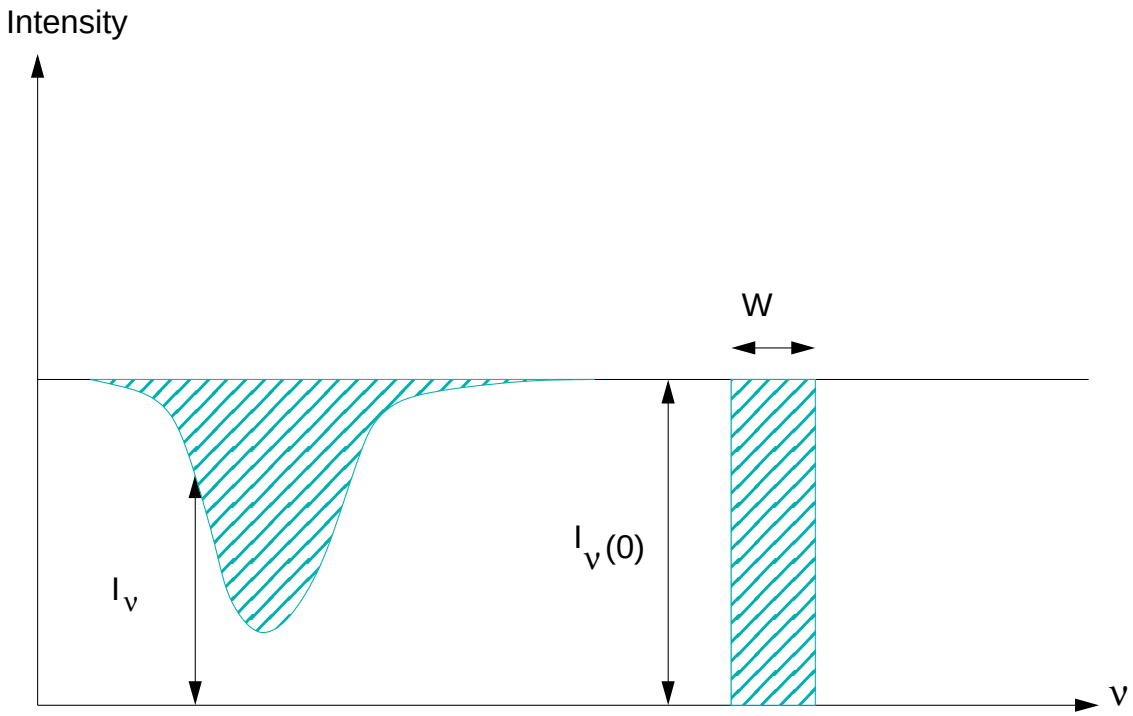

Figure 2.2 The area of an arbitrarily-shaped absorption line (left) can be represented by a rectangle with the same area. If the height of the rectangle is $I_\nu(0)$ then its width is W.

If the gas cloud absorbs light of frequency ν, the radiative transfer equation becomes $dI_\nu/d\tau_\nu = -I_\nu$ which is easily solved to obtain

$$I_\nu = I_\nu(0)e^{-\tau_\nu} \tag{2.10}$$

Now using the expression for equivalent width,

$$W = \int (1 - e^{-\tau_\nu}) d\nu. \tag{2.11}$$

If τ_ν is small (an optically thin or transparent medium), $W \approx \int \tau_\nu d\nu$.

The optical depth, τ_ν can be estimated assuming that photons run into other species (molecules, atoms, electrons) with cross section σ_ν. The total amount of absorption will be

$$\tau_\nu = \frac{\text{Number of Particles}}{\text{Area of beam of photons}} \times \text{Cross section} = N\sigma_\nu \tag{2.12}$$

where N is the column density of the cloud. The column density is the number density (number per volume) times the *physical* depth of a cloud, giving the number per perpendicular area.

Plugging $\tau_\nu = N\sigma_\nu$ into the optically thin expression for W,

$$W = \int N\sigma_\nu d\nu = N\sigma_0\Delta\nu \tag{2.13}$$

where σ_0 is the frequency-average cross section of a species averaged over a bandwidth $\Delta\nu$. Turning this around,

$$N = \frac{W}{\sigma_0\Delta\nu} \tag{2.14}$$

This expression gives a way to estimate the mass of a cloud. W is calculated from the spectra, σ_0 is either tested in a laboratory or estimated theoretically, and $\Delta\nu$ is the bandwidth of the receiver used. To find the entire mass of a cloud, we can integrate the column density N over its perpendicular area since, N(ℓ,b) is a function of both ℓ and b.

2.6 More on Turbulence

The study of turbulence in the interstellar medium is still an active area of research (Gustafsson et al., 2006), (Shore et al., 2006), and (Hily-Blant et al., 2008). It began with the observation that gas clouds have line widths too large to be explained by thermal broadening alone and so turbulence was suggested as a possible explanation. Line widths are essentially a measure of the breadth of an emission or absorption line, illustrated in Figure 2.3. Normally, large widths can be explained by Doppler broadening: hot particles have a range of velocities that redshift and blueshift to spread the light out over a range of wavelengths. Certain gas clouds, however, have such large line widths that they cannot be explained by thermal motions alone. For example, astronomers have found clouds that cannot be warmer than 10K as indicated by their spectra and high density. This temperature corresponds to $\mathrm{v}_{rms} \approx \sqrt{3kT/m_{CO}} \approx 0.09\ \mathrm{km\,s^{-1}}$, but the observed line widths are often $1 < \Delta v < 10$ km/s. While dynamical effects, such as gravitational collapse can add to line widths, astronomers have attributed the observed line widths to turbulent velocities (Lequeux, 2005).

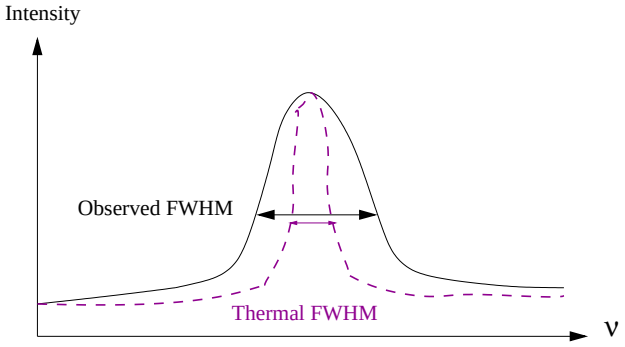

Figure 2.3 The width of a spectral line. This very broad-looking emission line can be described in terms of its Full Width at Half Maximum (FWHM). The FWHM for many gas clouds is too large to be explained by thermal motions alone, and must be attributed to other causes.

As described in detailed fluid dynamics calculations (Frisch, 1995), a fluid becomes chaotic and has vortices when the Reynolds number, R_e exceeds 100.

$$\frac{\text{advection}}{\text{diffusion}} = R_e = \frac{\text{LV}}{\nu} > 100 \tag{2.15}$$

where L and V are the characteristic scale and velocity of the flow and ν is the kinematic viscosity. This condition is required for turbulence, but it is easily met. An everyday example is in a swimming pool where ν=1/100 cm^2 s^{-1} (Frisch, 1995) so 1cm/s motion is all that is necessary to create turbulence around a 1cm-thick finger.

Turbulent velocities scale with the size of interstellar structures. Roughly $\sigma_v \propto L^{0.5}$ (Lequeux, 2005), where σ_v is the variance in turbulent velocity and L is the characteristic size of a turbulent region. This dependency reveals that the statistical properties of turbulence are scale-invariant, in other words, fractal in nature. While the actual shape of turbulence looks dissimilar at different size scales, the general statistical features remain the same.

2.6.1 Intermittency

Turbulence can sometimes depart from fractal behavior. When this occurs, the technical term is called intermittency. Figure 2.4 shows a possible scheme for intermittency. In this form of intermittency, smaller-scale eddies do not fill the full volume of the cloud the way larger-scale ones do. This discrepancy with volume-filling means that the statistical properties of the gas are no longer scale-invariant. Aside from the interesting consequences this may have to theoretical turbulent models, it has a direct consequence for interstellar clouds; the energy from large-scale turbulence becomes concentrated in a specific area of the cloud. With the concentration of energy, the cloud is heated in certain spots far more than if the energy were evenly dissipated throughout the volume. This is the kind of heating we search for in Clump 1 and Clump 2 using a technique called velocity centroids.

2.6.2 Velocity Centroids

Turbulence is difficult to measure in astronomy because of the vast distances involved. For anything farther out than our Sun's nearest neighbors, the third dimension (depth) is elusive because we cannot significantly move our vantage point. This is one of the classic difficulties in astronomy. Velocity is also hard to measure because proper motion (motion that is perpendicular to our line of sight) is often too slow for observation. Radial motion, however, is much easier, via Doppler shifts. To summarize, one component of position is essentially unavailable in (r_1, r_2, r_3) and two components (the perpendicular plane) of velocity (v_1, v_2, v_3) are unavailable. The missing information makes it hard to measure turbulence, but it is still possible.

The velocity centroids technique is a way to analyze turbulent motion statistically (Pety & Falgarone, 2003) knowing only radial velocity. The first step is to calculate the "velocity centroids" along every line of sight.

$$v_{\text{centroids}}(\ell, b) = \frac{\int I_\nu(\ell, b, v) v dv}{\int I_\nu(\ell, b, v) dv} \tag{2.16}$$

The second step is to measure differences in centroid velocities. These differences are called velocity increments and are calculated for a specific length. That is, each coordinate pair (ℓ_1,b_1) is compared to another pair (ℓ_2,b_2) separated by a distance l. This is repeated for all the feasible points within a region of interest. Care must be taken to avoid double-counting pairs. The third step is to compile the velocity increments into a Probability Distribution Function (PDF) by binning velocity increments and plotting a histogram.

Figure 2.5 shows several PDFs for four different velocity increment scales l = 3,6,9 and 12 pixels. The distributions at small l show non-Gaussian "wings" whereas the PDF at largest l is very close to Gaussian. From experimental laboratory results and numerical models of fluids,

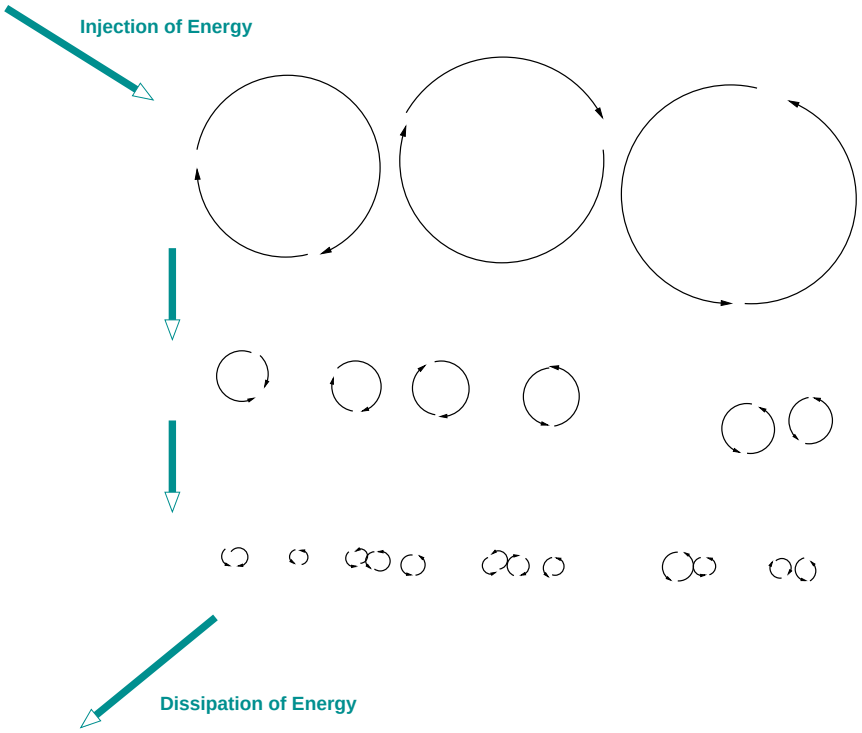

Figure 2.4 The energy from large eddies can be concentrated in very small locations in space. Thus, parts of this cloud could be heated very strongly. Compare this illustration to Figure 2.1, where the smaller eddies fill the full volume of the cloud—conserving scale-invariance. In the above figure, the statistical properties of the turbulence change with scale size, so they are "intermittent."

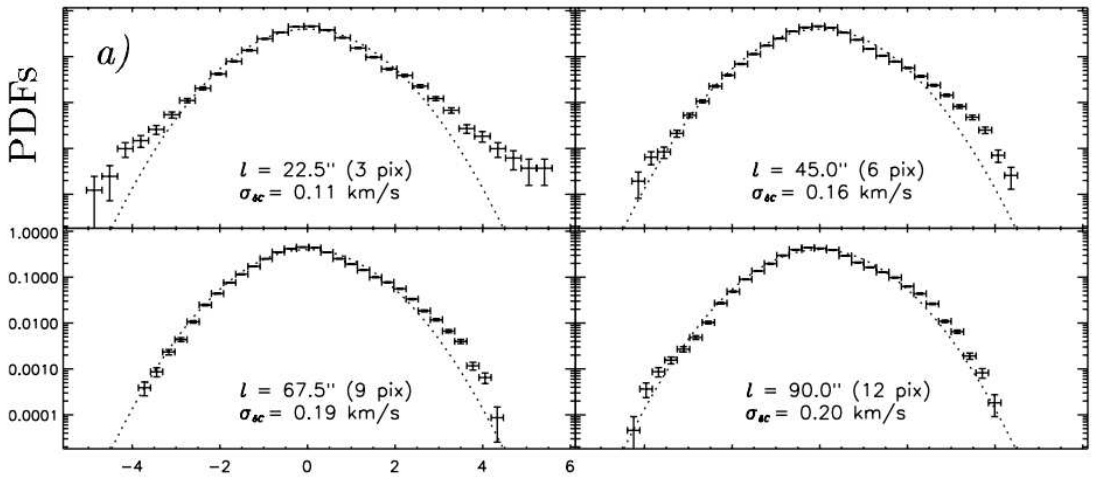

Figure 2.5 Velocity increments PDF from Pety & Falgarone (2003). For large increments the PDF is approximately Gaussian and for small increments the PDF has "wings" where the data departs from a Normal (Gaussian) PDF. The Gaussian fits are plotted as dashed lines.

non-Gaussian "wings" indicate intermittency in the fluid being described (Lis et al., 1996). The

wings are a sign of strong vorticity[2].

The velocity centroids technique is not perfect. One problem is that it only works for sub-sonic turbulent velocities (Lazarian, 2008). Other techniques, like Velocity Coordinated Spectrum (VCS), as described by Lazarian (2008), can handle super-sonic turbulent velocities. Another problem is that the technique does not work well in star-forming regions, where collapsing clouds can change the PDFs (Pety & Falgarone, 2003). Given these problems, velocity centroids does not guarantee that turbulent dissipation is present, but instead indicates that it is likely.

[2]vorticity = $\vec{\nabla} \times \vec{v}$

Chapter 3

Cloudy

3.1 Calculations

Cloudy calculations are based on the assumption of a steady-state cloud. For all species, the rate at which particles enter a state equals the rate they leave. This is expressed in a balance equation:

$$\frac{\partial n_i}{\partial t} = \sum_{j \neq i} n_j R_{ji} + \text{Source} - n_i \left(\sum_{j \neq i} R_{ij} + \text{Sink} \right) = 0 \ \ \text{cm}^{-3}\text{s}^{-1} \tag{3.1}$$

where the species of interest has density n_i. The rate of change of this density is zero because all species transitioning from and into state j balance with the Source and Sink.

Equation 3.1 holds for all species i, so Cloudy must solve as many equations as there are species. They are coupled equations because chemical reactions, photon absorption and emission can convert one species to another. Cloudy attempts to solve them all, and thus calculate every population level for every excited state of every species (Ferland, 2003).

Cloud modeling is more complicated than just solving coupled equations, though. The equations must be correct. Most of them depend on physical constants like cross-sections of interactions. For example, the interaction of an electron and a CO molecule depends on their relative velocity and positions. Rather than try to quantum-mechanically predict the probability these two species interact, Cloudy keeps it as a constant—there are way too many complicated interactions to calculate by first principles. Other constants, like Einstein A and B coefficients, which describe the rates of spontaneous and stimulated emission and absorption, must similarly be entered in the database. Atomic data are constantly being updated and changed as theory and observation improve.

Even if all the coupled equations are set up perfectly and solved, Cloudy must still correctly handle the radiative transfer through a cloud. Some photons will escape readily, without interacting with atoms. Other photons are easily absorbed by the same processes that create them. The latter case is optically thick emission ($\tau > 1$). Cloudy solves the radiative transfer with the escape probability method (Ferland, 2003).

3.2 Input

There are only three inputs needed to predict a resulting infrared spectrum:

- Incident continuum
- Chemical/Dust abundances
- Density structure

From these few parameters, Cloudy can predict thousands upon thousands of line intensities, temperatures, and a resulting spectrum.

3.3 Continua

Cloudy calculates several different continua. As seen in Figure 3.1, the incident continuum from an ionizing source is reflected, absorbed and transmitted by the cloud. An observer will see some attenuated form of the original spectrum plus a diffuse spectrum that originates from the cloud itself. Reflected photons can be important in calculations because they influence gas conditions within the cloud and also in nearby clumps of material. For our models, the diffuse contiuum is the key concern.

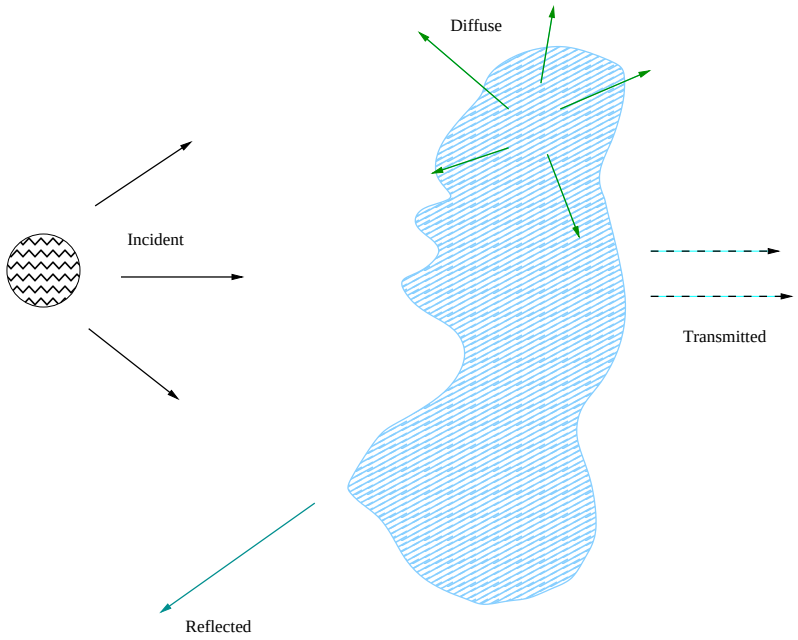

Figure 3.1 Schematic of the various continua calculated by Cloudy.

Chapter 4

Results and discussion

4.1 Data

All of the data used in this paper come from outside sources—Martin et al. (2009) (in preparation), Bally et al. (1987), and Bally et al. (1988). These papers describe the nature of the data; hence, we skip the details of how the spectra were obtained, compiled, reduced, and processed. Instead we describe our analysis. This chapter begins with a brief introduction to data cubes, discusses how we studied them, and concludes with models that fit the data.

4.1.1 Data Cubes

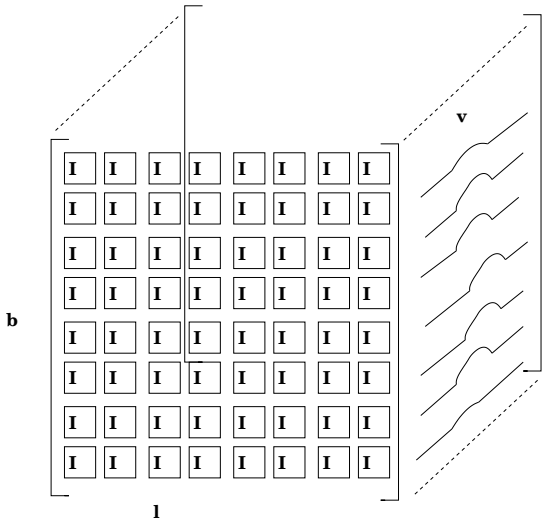

Figure 4.1 This data cube's dimensions are ℓ, b, and v. Each box in the cube corresponds to an intensity, I(ℓ,b,v). A normal camera produces a rectangular array of data, but a spectrometer can create a data cube. Each (ℓ,b) position has a spectra (an intensity vs. wavelength plot) as drawn in on the right face of the cube. For this paper, wavelength is converted to velocity by the classical redshift formula, $\lambda(\text{observed}) = \lambda(\text{motionless}) \times (1 + v/c)$

Martin et al. (2009) took observations of Clump 1 and 2 from the South Pole telescope, Antarctic Submillimeter Telescope and Radio Observatory (AST/RO). They obtained spectral maps at several frequency bands ranging from 220 GHz to 806 GHz at the South Pole, including four important interstellar emission lines: CO $J = 4 \rightarrow 3$, CO $J = 7 \rightarrow 6$, ^{13}CO $J = 2 \rightarrow 1$ and

[C I] $^3P_1 \rightarrow {}^3P_0$. The first three CO lines are rotational transitions introduced in §2.1 while the [C I] $^3P_1 \rightarrow {}^3P_0$ line is an atomic transition.

The instruments at the AST/RO were used to make data cubes of the above-mentioned emission lines. Data cubes consist of two spatial positions, ℓ, b and one spectral dimension, v. Figure 4.1 shows how the combined data may be visualized. Obviously, the number of pixels in the ℓ, b, and v directions do not have to be equal, so it is really a "data rectangular prism," but data cube is easier to say. The v dimension is a proxy for depth, especially when gas stretches along a velocity gradient, but it does not exactly correspond to distance.

Martin et al. (2009) made color contour plots to help visualize the cubes. Figure 4.2 shows ℓb "slices" of the data cube that are perpendicular to the line of sight. Each slice shows an average brightness for a range of velocities.

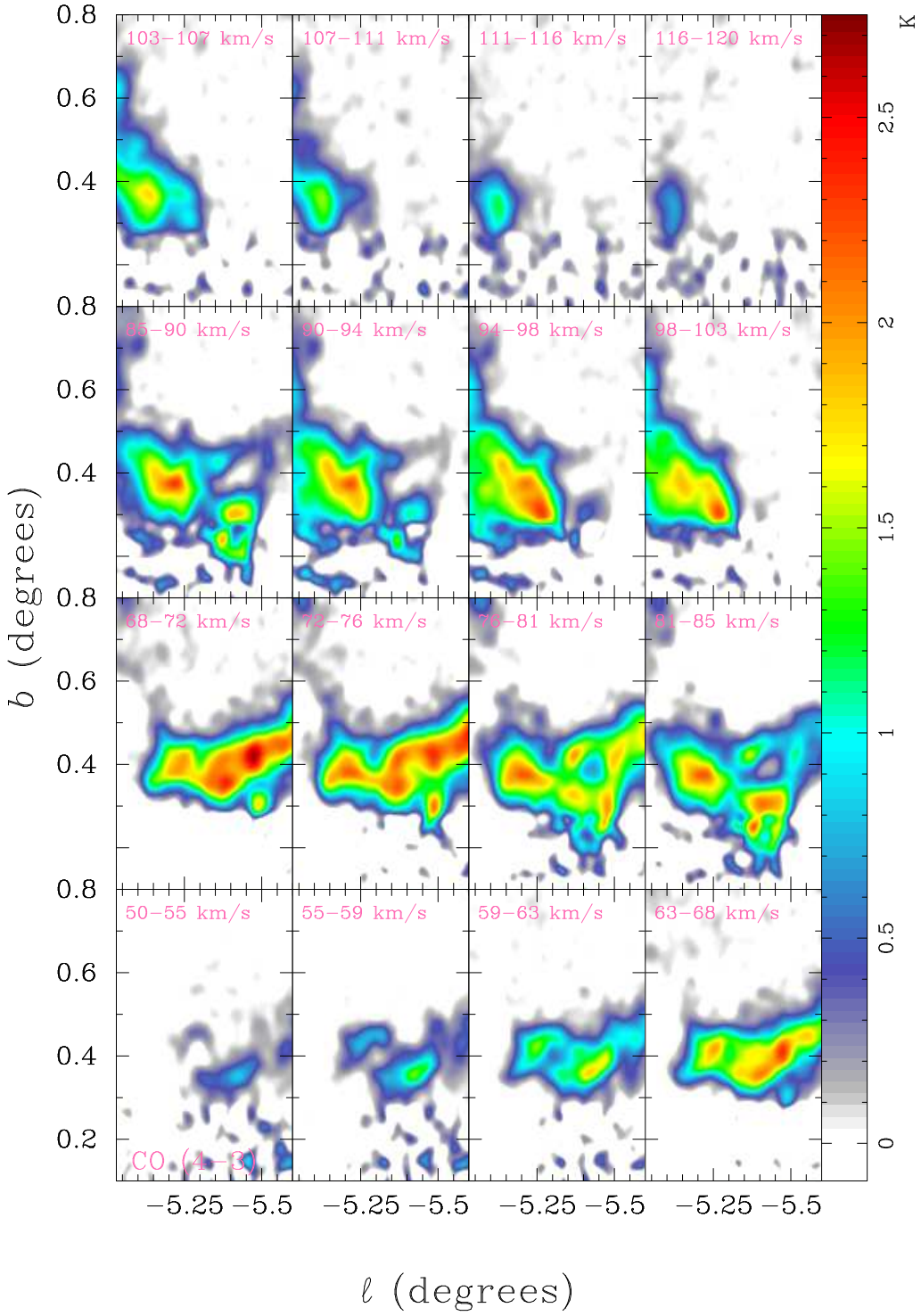

Figure 4.2 Data cubes can be represented by a series of "slices" as shown above. Each slice shows the intensity as averaged over a smaller range of velocities. The intensity is represented by color—red being the highest antenna temperature, T_A^* (see §2.1 for a description) and white being the lowest. The x-axis is Galactic longitude and the y-axis is Galactic latitude. Slices can also be made in other directions to help indicate velocity structure.

4.2 Characterizing the Turbulence

As described in the Introduction, Clump 1 and Clump 2 do not have any significant star clusters in the area, so we investigated the possibility that they are heated up by other sources. One possibility could be the radiation from the accretion disk around the Milky Way's supermassive black hole, but it is unlikely to be very powerful. Therefore, we explore the possibility of turbulent heating. This kind of energy comes from gas kinematics—the collisions and interactions of the gas with the Galactic bar and each other. The following analysis helps indicate whether turbulence can be a source of heating for each clump.

Data cubes lend themselves to analysis of dynamics because they contain information on both position and velocity. We took advantage of the data cubes for Clump 1 and 2 by exploring velocity centroids within them. Turning a cube into a velocity centroid map is easy, using equation 2.16. We then performed the method described in §2.6.2, modifying the Interactive Data Language (IDL) script `clplot` (Williams et al., 1994) to aid our calculation.

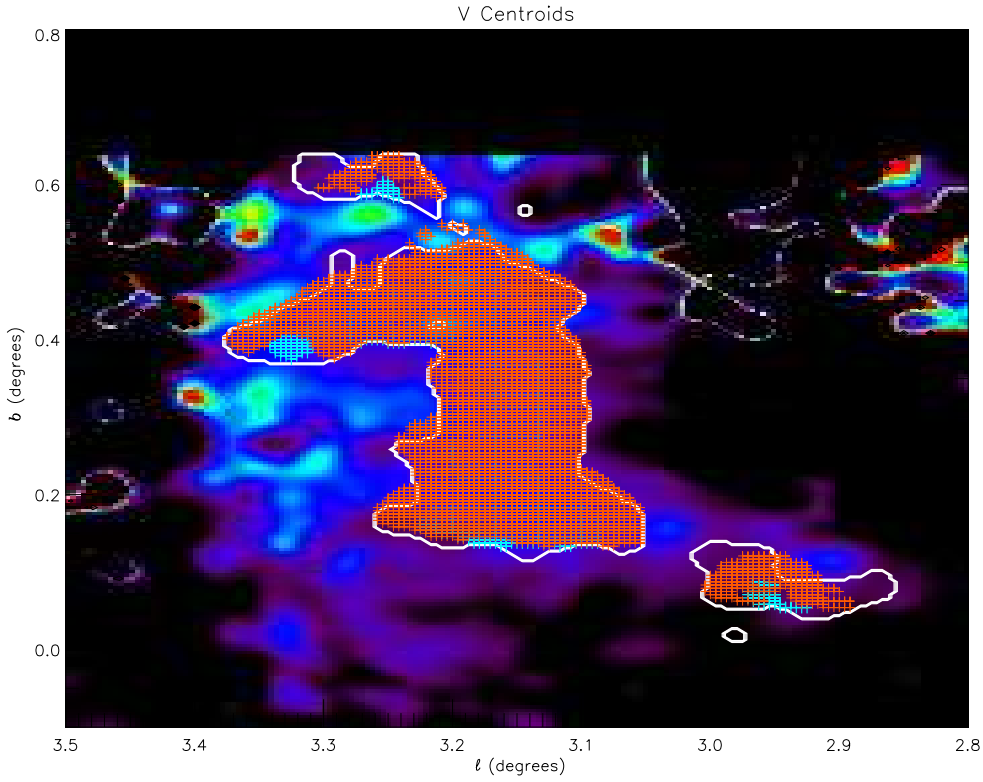

Figure 4.3 The velocity centroids of Clump 2, shown in this color contour plot, reveal that the centroids have little correspondence with the integrated brightness. This is emphasized by the white outline, which surrounds the brightest CO $J = 4 \rightarrow 3$ emission. Overlaid on this plot are two sets of points. The inner blue points are the base points of velocity increments. For each of these blue base points, a semi-circle of comparison points is drawn in red. The *base* points were restricted to the innermost region so that the *reference* points would be roughly within the brightest CO $J = 4 \rightarrow 3$ emission (the white boundary). Compare this plot with the CO $J = 4 \rightarrow 3$ emission in Figure 1.7 to see differences between centroids and integrated brightness.

We first chose the appropriate ring of reference points with respect to a base point. This is pictured in Figure 4.4(a), where the + signifies a base point. A semicircle of pixels surrounds this

base point at a fixed pixel radius. This pattern is repeated for the whole cloud, as seen in the full maps of inner and outer pixels in Figure 4.3.

Velocity centroids can be subtracted between reference and base points to make so-called "velocity increments." In mathematical terms, the velocity increments are $\delta v(l) = v(\text{base}) - v(\text{reference}) = v(\vec{r}) - v(\vec{r} + \vec{l})$ where $\vec{l}$ is the "increment," with magnitude l. We calculated these increments for several different l, and the results are seen in Figures 4.4(b), 4.5(b), 4.6(b). These figures show the normalized histograms, or Probability Distribution Functions (PDFs) for all the velocity increments.

4.2.1 Clump 2 Increments

As described in §2.6.2, departures from Gaussian PDFs can indicate enhanced vorticity. In Clump 2, enhanced vorticity is seen as "wings," where the PDFs are greater than a Normal distribution far from the mean. Figure 4.6(b) shows the strongest wings because it is the smallest velocity increment, l. In contrast, when $l = 12$ pixels, as in Figure 4.4(b), the PDF is very close to Normal. We note that the plots are in log-log space, so the Gaussian distribution looks dome-like, rather than bell-like.

Careful inspection of the pixel map in Figure 4.5(a) shows that the 8 pixel increments were chosen slightly differently from the 12 pixel ones. They exclude the leftmost points in the semicircle to avoid double-counting. 12 pixel semi-circles, however, do not overlap as frequently as the 8 pixel ones, so they do include the leftmost semicircle point. Either way, the PDFs were not very strongly affected by this single point. Following the logic of the 8 pixel increments, the $l = 4$ pixel maps also exclude the leftmost points.

The progression from l=12 pixels down to l=4 pixels in Figures 4.4(b), 4.5(b), and 4.6(b) shows a pattern of increasingly strong "wings." While the velocity centroids method does not provide unambiguous proof, it is a strong indicator that small-scale vorticity is more prominent than large-scale vorticity. Such dependence on increment size l is a departure from the general observation that turbulence is scale-invariant (Frisch, 1995). Hence, the energy from large-scale motions may be concentrated in certain brighter portions of Clump 2. If the turbulence was truly scale-invariant, we would expect no departure from a Gaussian PDF. Instead, we see that large scale motions probably funnel their energy to the brighter regions of Clump 2, while less energy is dissipated to the dimmer regions.

The size scales referred to previously as pixels can easily be converted to distances. The plate scale is 0.0042°/ pixel, so at a distance of 8500pc, l=4pixels corresponds to 2.5pc. 12 pixels amounts to 7.5pc. This means that the departure from scale-invariance occurs for eddies around 3 parsecs in size.

4.2.2 Clump 1 Increments

In contrast to Clump 2, Clump 1 is probably not heated by turbulent dissipation. 1's PDFs are lobsided and pretty constant with scale size. If there is turbulent motion in Clump 1, it obeys more classical fractal behavior because the statistical properties do not depend on the size of turbulent eddies. Without intermittency, the energy added to any one location in Clump 1 cannot be very significant, as described in §2.6.

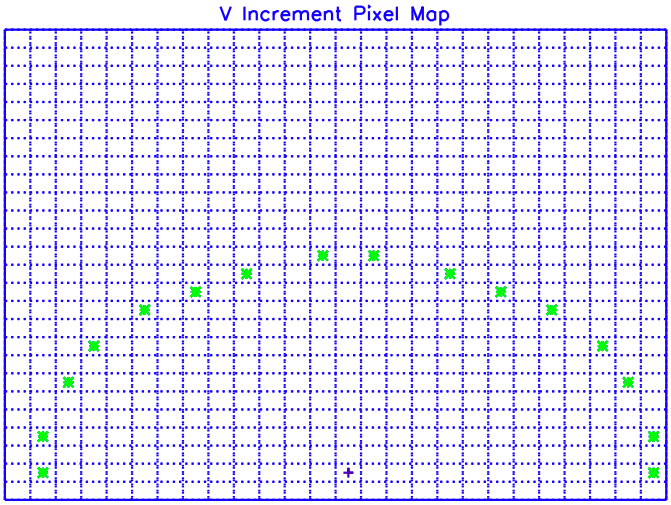

(a)

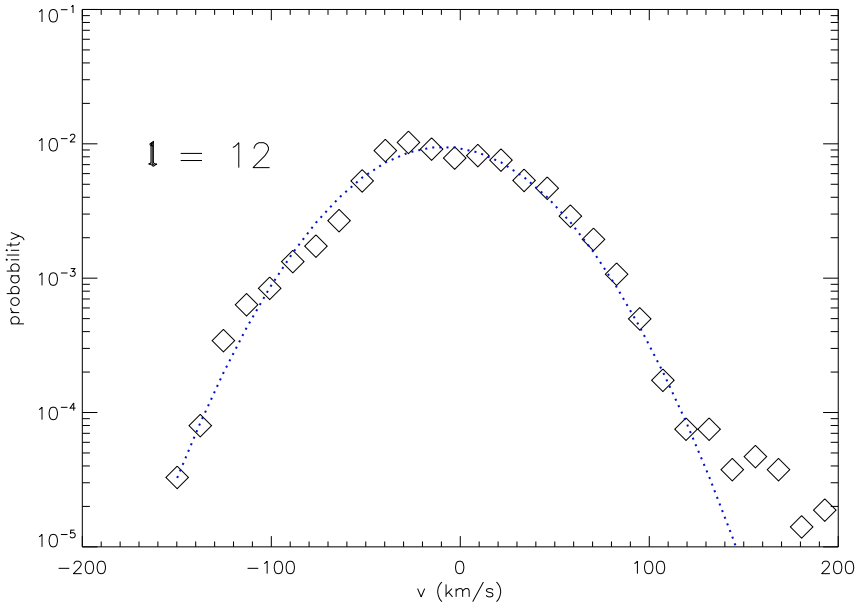

(b) PDF

Figure 4.4 The pixel map, (a), shows a base point marked with a plus. Surrounding this base point, with a radius of 12 pixels is a set of reference points. Velocity increments were calculated between the base and references and then repeated for the entirety of Clump 2. The histogram of the increments is seen in (b) and very closely fits a Gaussian distribution.

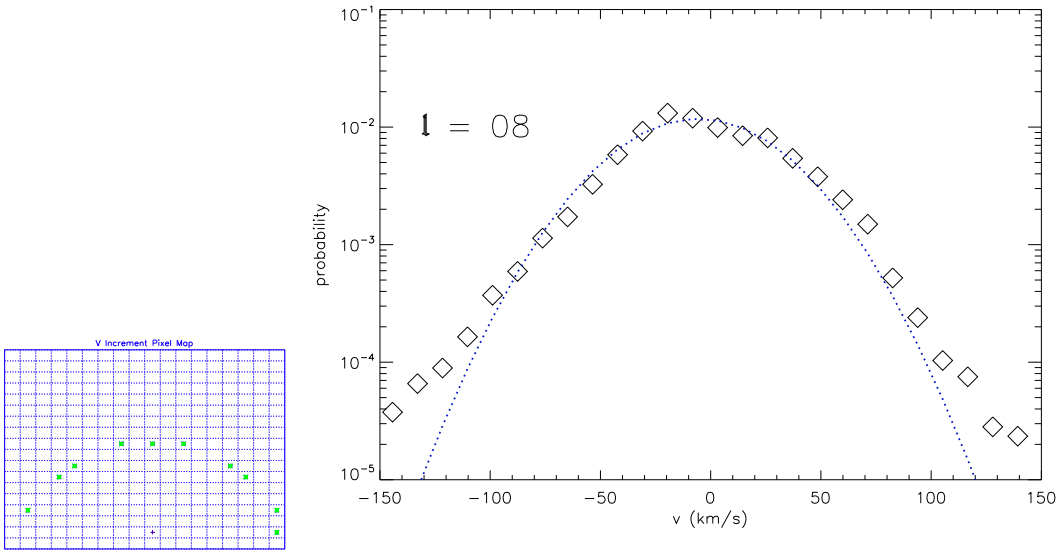

(a) (b) PDF

Figure 4.5 The pixel map, (a), reveals that the leftmost reference point is excluded for l=8 pixels and smaller. At this l, non-Gaussian "wings" begin to emerge in the PDF for Clump 2 seen in (b).

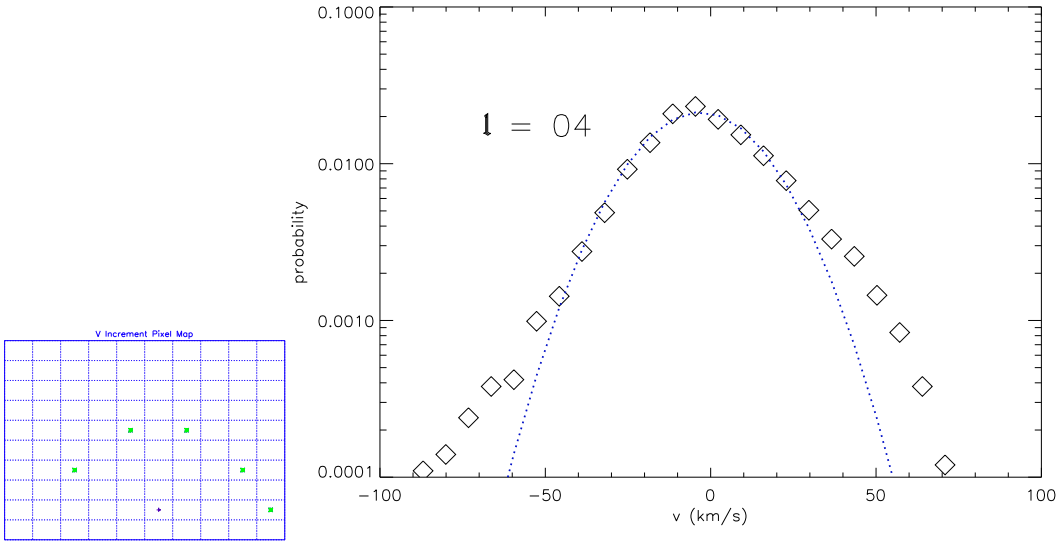

(a) (b) PDF

Figure 4.6 Figure (b) shows pronounced non-Gaussian "wings" where the histogram departs from a Normal curve. This is a sign of enhanced vorticity at these smaller scales. While it is not a proof, the "wings" indicate that Clump 2 might be heated by turbulent dissipation.

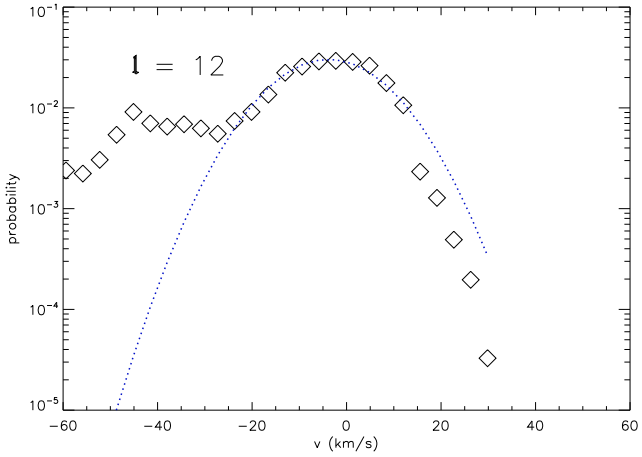

(a) PDF

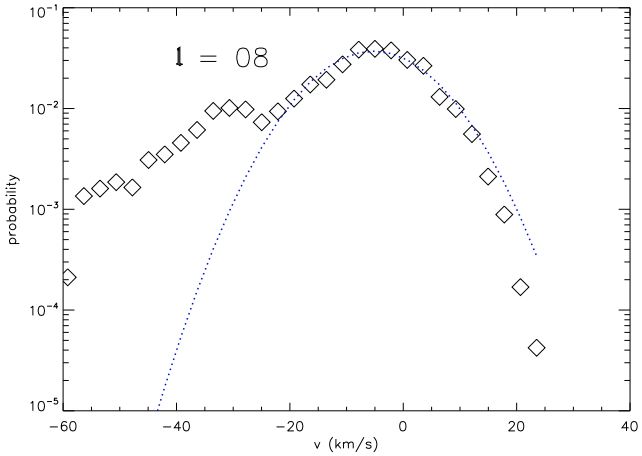

(b) PDF

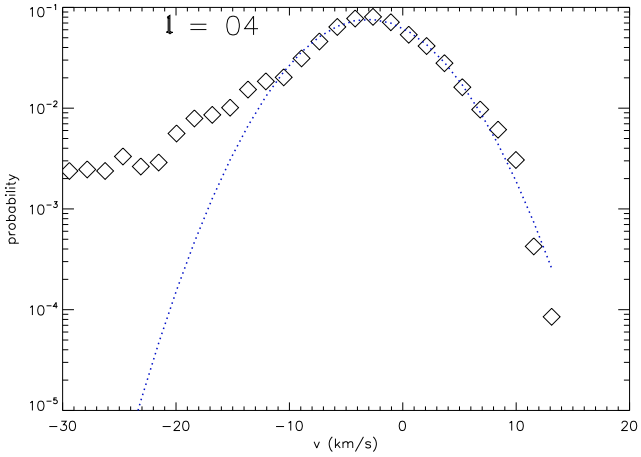

(c) PDF

Figure 4.7 Clump 1 PDFs do not show significant dependence on scale, l. It is less likely that Clump 1 is heated by turbulent dissipation the way Clump 2 is. The pixel maps used for calculating the increments in Clump 1 are identical to those in Figures 4.6(a), 4.5(a), and 4.4(a).

4.3 Models

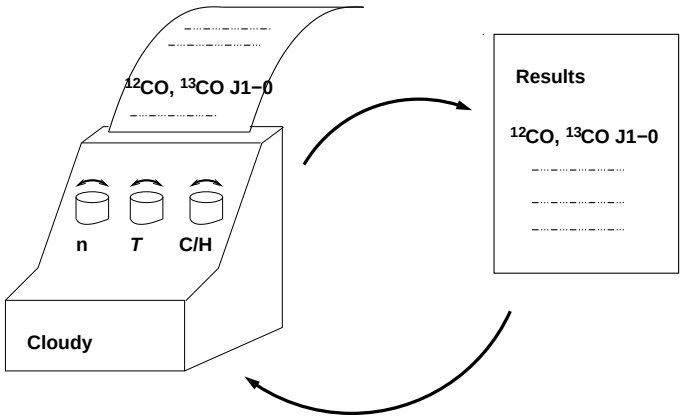

Figure 4.8 Cloud model parameters vs. actual measurements. Each model has a set of parameters, pictured as knobs. When the model is run, it makes a set of intensity predictions. The results are compared to the data and then the model is run again tweaking the knobs slightly. If the predictions get closer to the data, we continue moving the knobs as we were, otherwise we try different parameters. Then the model is run again and the cycle is repeated until some threshold is reached—error, number of iterations or time could be the stopping points.

Numerical models were used to estimate physical properties—temperature and density—of the Inner Galaxy Gas Clumps (IGGCs) described in §4.3.1. For each IGGC, CO $J = 4 \rightarrow 3$, ^{13}CO $J = 2 \rightarrow 1$, CO $J = 7 \rightarrow 6$ and [C I] $^3P_1 \rightarrow {}^3P_0$ antenna temperatures were used to constrain the models. Since there are still uncertainties about the calibration of these T_A^*, we used ratios between these emission lines because calibration errors are divided out this way. Figure 4.8 shows how these models are then adjusted to fit the data.

4.3.1 Inner Galaxy Gas Clumps (IGGCs)

As evident from Figures 4.2, 1.7, 1.6, Clump 1 and Clump 2 are full of knots and inhomogeneities. They are really composed of sub-clumps, dubbed IGGCs 1 through 24. Each IGGC was identified by the `clumpfind` algorithm (Williams et al., 1994), which chose compact and spherical structures within the Bania macro-clumps, 1 and 2.

These smaller structures are easier to model as separate pieces rather than as a whole. In the models, we used average intensities for each IGGC calculated by Martin et al. (2009). These average intensities were converted to antenna temperatures, T_A^* as described in 2.1.

4.3.2 Large Velocity Gradient (LVG) Models

Independently from Cloudy, Martin et al. (2009) used a LVG model to predict cloud conditions. The LVG approximation gives a solution for the radiative transfer equation. As derived in Lequeux (2005), the mean intensity (I_ν averaged over all directions) is

$$\int I_\nu d\Omega = (1 - \beta(\tau))S(\tau) \tag{4.1}$$

where β is the photon escape probability. When taking into account the velocity gradient, β turns out to be

$$\beta = \frac{1 - e^{-3\tau}}{3\tau} \tag{4.2}$$

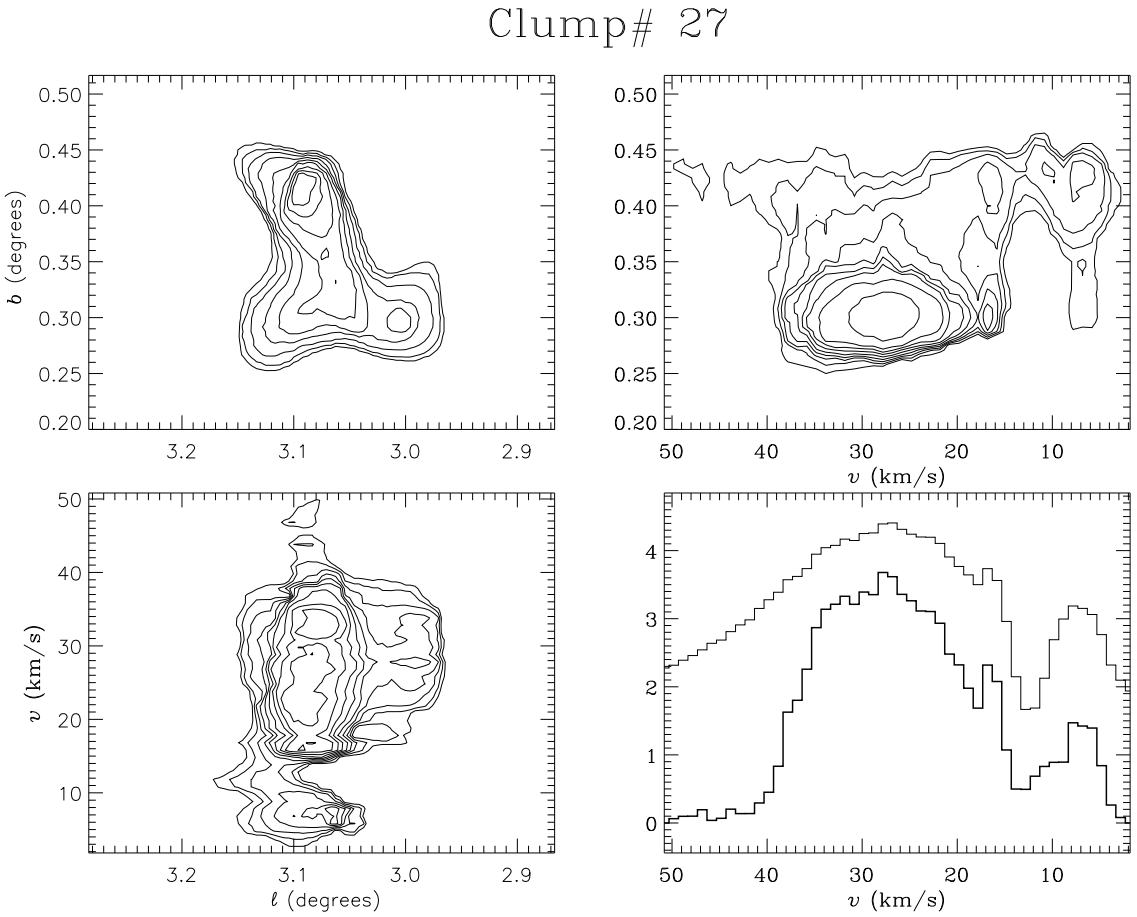

Figure 4.9 `Clumpfind` identifies IGGCs within Bania Clump 1 and Clump 2. It identified over 55 sub-clumps within Bania Clump 2. This is sub-clump #27, which was later named IGGC 15. These contour plots give different views of the cube pictured in Figure 4.1. Top Left gives the integrated emission as viewed from earth or the ℓb plane. Top Right gives the vb plane. Bottom Left gives the ℓv plane, where the same v $\approx$ 48 km/s chunk can be seen separated from the IGGC as in Top Right. Finally, Bottom Right shows the average spectrum (intensity bin vs. v) for the IGGC on the bottom and the entire Bania Clump 2 on the top.

where τ is the optical depth. Equation 4.2 may be substituted into equation 4.1 thus presenting a solution to the radiative transfer equation. This is how the intensity varies with optical depth.

4.3.3 Forced Temperature Models

In order to estimate gas temperature, we made cloud models of fixed temperatures. The following parameters were used in the models:

- Plane parallel mode (see Figure 1.3)
- Cosmic Ray Heating, no photo-ionization
- Forced Temperature
- Constant Hydrogen Density
- ^{12}CO / ^{13}CO = 24.0

- Optimized to observed line ratios
  (CO $J = 2 \rightarrow 1$)/(CO $J = 4 \rightarrow 3$)
  ([C I] $^3P_1 \rightarrow {}^3P_0$)/(CO $J = 4 \rightarrow 3$)

Plane parallel models assume a uniform and flat shell of gas, as pictured in Figure 1.3. Cosmic ray heating is the energy added by fast-moving particles known to pervade the Galaxy. The total heating by cosmic rays is pretty small for our cloud densities. In models with cosmic rays as the only heating source (no X-Rays, UV photons, or dynamical heating), the temperature barely rose above a few K. If cosmic rays are at background levels, as is found in the solar neighborhood, they only heat a cloud to 2.9K. If they are at 100 times this rate as predicted by Oka et al. (2005) in the GC (See § 2.2.2), the cloud is still only 5K. While a typical cloud has a hot star (see Figures 3.1), these models ignore stellar heating and instead force the cloud to be at a specific temperature. For simplicity, the entire IGGC is assumed to be the same density, so there are no knots of high density or gaps between the clouds' components.

Table 4.1 shows the optimization routine used for IGGC 04. From the AST/RO data, the intensity ratios ([C I] $^3P_1 \rightarrow {}^3P_0$)/(CO $J = 4 \rightarrow 3$) and (CO $J = 2 \rightarrow 1$)/(CO $J = 4 \rightarrow 3$) were both 0.27. The first guess (iteration 0) was $n = 10^{3.6}$ and T=$10^{1.6}$. These yielded ratios of 0.23 and 0.15. Density is then adjusted for iteration 1, which had much worse predictions as evidenced by larger χ^2. Iteration 2 goes back to the initial n and this time, temperature is varied. This process is continued until Cloudy has either converged on a result or reached the maximum number of iterations.

Table 4.1 Optimizing IGGC 04. The density n and temperature T are varied from the initial guess until χ^2 (error) is minimized.

Iteration	χ^2	log(n)	log(T)	[C I] $^3P_1 \rightarrow {}^3P_0$ [a]	CO $J = 2 \rightarrow 1$ [b]
0	3.82e+03	3.60	1.60	0.23	0.15
1	5.11e+11	4.60	1.60	0.00	0.04
2	9.00e+08	3.60	2.60	0.00	0.03
3	3.48e+09	2.60	2.60	228.06	0.07
4	3.55e+06	3.10	2.35	7.50	0.07
5	4.70e+08	3.10	1.35	83.98	0.50
6	1.58e+06	3.23	1.66	5.13	0.16
8	1.45e+05	3.26	1.99	1.62	0.09
10	3.31e+04	3.53	1.86	0.15	0.08
12	4.72e+04	3.72	1.60	0.07	0.13
14	2.24e+05	3.60	1.35	2.10	0.41
16	1.36e+05	4.10	1.23	0.04	0.54
18	8.49e+03	3.66	1.41	0.63	0.29
20	3.63e+02	3.69	1.45	0.34	0.25
22	9.99e+02	3.69	1.50	0.22	0.20
24	2.50e+02	3.77	1.41	0.22	0.27
26	1.55e+02	3.75	1.39	0.31	0.30
28	5.41e+01	3.73	1.42	0.30	0.26
30	2.42e+03	3.79	1.42	0.16	0.25
32	4.73e+02	3.74	1.39	0.35	0.30
34	1.88e+02	3.76	1.42	0.23	0.27
36	6.82e+01	3.74	1.41	0.30	0.28
38	8.65e+00	3.75	1.42	0.26	0.27

[a] The [C I] $^3P_1 \rightarrow {}^3P_0$ line intensity is normalized with respect to CO $J = 4 \rightarrow 3$. The observed intensity ratio was ([C I] $^3P_1 \rightarrow {}^3P_0$)/(CO $J = 4 \rightarrow 3$) = 0.27
[b] Normalized as in Note [a] . The observed value was 0.27

Cloudy also predicts other properties of a cloud. The following list shows a few of the results for IGGC 04, using the optimal density and temperature:

- Phases of hydrogen:
  98% atomic H, 2% molecular H_2, $\ll 0.1\%$ ionized H^+

- C II intensity = 0.002 in units of CO $J = 4 \rightarrow 3$
  This could be confirmed or refuted by the Herschel Space Observatory

In the same way as for IGGC 04, we made models to fit all of the IGGCs. The compiled results are seen in Table 4.2 as compared with the LVG models. The LVG method consistently predicts higher temperatures, with the exception of IGGC 23 and 24. This may be due to the inclusion of the CO $J = 7 \rightarrow 6$ in the LVG model and exclusion of it in Cloudy models. See § 4.4 for more on this point. $n(H_2)$is also lower in the Cloudy models because the Cloudy models consist of (98%) atomic hydrogen. The LVG models assume entirely molecular hydrogen, H_2.

Table 4.2 LVG vs. Cloudy Results

	ℓ °	b deg	$v_{\rm LSR}$ km/s	R2[a]	R3[b]	T_{LVG} K	n_{LVG} cm^{-3}	T_{Cloudy} K	$n(H_2)_{Cloudy}$ cm^{-3}	$n_{HCloudy}$ cm^{-3}
IGGC1	-5.37	0.37	71.1	0.17	0.29	130.2	2.53	33.1	2.07	3.75
IGGC2	-5.47	0.42	70.0	0.19	0.30	128.3	2.53	29.0	2.01	3.81
IGGC3	-5.58	0.45	73.1	0.16	0.28	131.2	2.53	34.7	2.08	3.73
IGGC4	-5.44	0.30	80.7	0.27	0.27	130.2	2.53	23.9	1.92	3.93
IGGC5	-5.38	0.24	84.4	0.26	0.26	94.5	2.67	23.0	1.90	3.95
IGGC6	-5.21	0.37	82.3	0.44	0.52	55.1	2.77	19.6	1.80	3.98
IGGC7	-5.25	0.31	97.5	0.54	0.46	43.8	2.93	17.5	1.73	4.03
IGGC8	-5.52	0.23	51.2	0.29	0.00	107.7	2.84	N.A	N.A	N.A
IGGC9	-5.25	0.08	52.9	0.39	0.09	57.9	3.29	18.5	1.75	4.18
IGGC10	-5.07	0.78	77.8	0.14	0.86	91.7	3.08	43.1	1.96	3.51
IGGC11	-5.31	0.15	83.5	0.40	0.40	49.4	3.20	19.6	1.80	3.98
IGGC12	-5.18	0.13	88.9	0.30	0.70	48.5	3.10	24.0	1.88	3.81
IGGC13	-5.08	0.15	92.5	0.40	0.60	56.9	2.89	20.0	1.80	3.93
IGGC14	-5.46	0.15	111.0	0.13	0.13	41.0	3.22	38.1	2.21	3.78
IGGC15	3.07	0.35	25.0	0.20	0.25	124.6	2.55	28.7	2.02	3.84
IGGC16	3.30	0.43	41.3	0.09	0.06	132.1	2.53	51.9	2.39	3.76
IGGC17	3.28	0.61	44.7	0.08	0.08	133.0	2.55	60.9	2.38	3.70
IGGC18	3.22	0.57	75.2	0.06	0.11	N.A	N.A	231.	1.72	3.44
IGGC19	3.16	0.40	83.2	0.08	0.08	134.0	2.53	57.4	2.37	3.71
IGGC20	3.21	0.61	99.9	0.06	0.06	N.A	N.A	80.7	2.40	3.67
IGGC21	3.28	0.59	102.0	0.00	0.09	N.A	N.A	N.A	N.A	N.A
IGGC22	3.06	0.16	146.0	0.24	0.31	98.3	2.89	21.9	1.87	3.99
IGGC23	3.35	0.39	147.0	0.05	0.20	131.2	2.53	148.0	2.16	3.55
IGGC24	3.15	0.77	107.0	0.05	0.27	132.1	2.53	368.0	1.37	2.57

[a] R2 is the ^{13}CO $J = 2 \rightarrow 1$ / CO $J = 4 \rightarrow 3$ emission line ratio.
[b] R3 is the [C I] $^3P_1 \rightarrow {}^3P_0$ / CO $J = 4 \rightarrow 3$ emission line ratio

Figures 4.10 and 4.11 plot out the data in Table 4.2 to see visually how the models differ. Each figure includes two Cloudy runs, at different abundances of Carbon. The real ratio of C/H is an uncertain number. The LVG model uses log(C/H)=-3.62, so this is the most relevant for comparing LVG and Cloudy. If the real ratio is smaller, like 10^{-4}, the average density drops by 30% and the average temperature increases by 5%.

4.3.4 Ultra-Violet Models

While the Forced Temperature models can be used to predict temperature and density, they do not explain how a cloud is heated. To make a more realistic model, some source of heating must be specified. We made Ultra-Violet (UV) models where the primary source of heat was a hot star, emitting strong UV radiation. Besides this star's radiation, the models are identical to the Forced Temperature models with respect to metallicity[1], cosmic rays flux, and observational constraints.

[1]Metallicity describes how many metals are present in an astrophysical environment. In astronomy a "metal" describes an element with an atomic number greater than 2. Metallicity is often measured by 12+log(O/H) where O/H represents the fractional abundance of oxygen with respect to H.

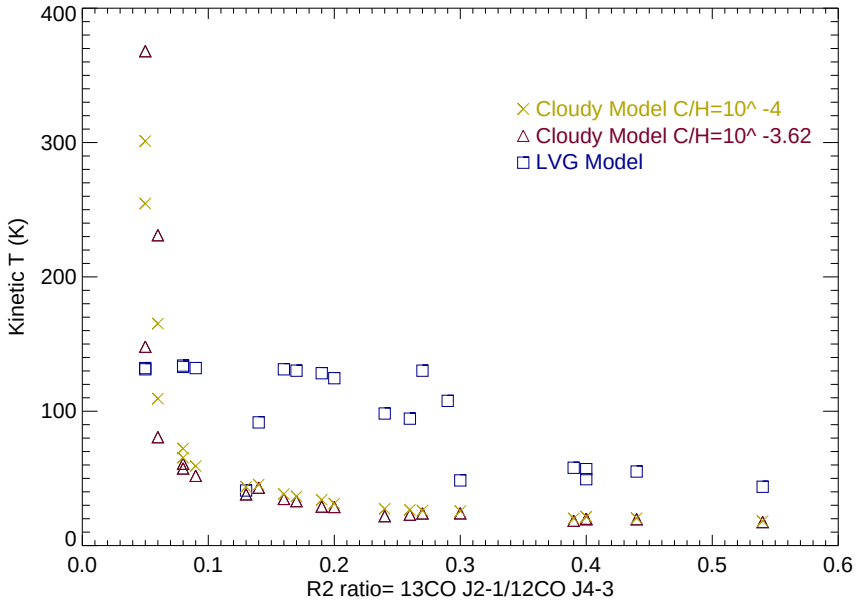

Figure 4.10 Cloudy vs LVG models. The Cloudy Forced temperature models show a dependence on the R2 ratio that puts them below the LVG predictions.

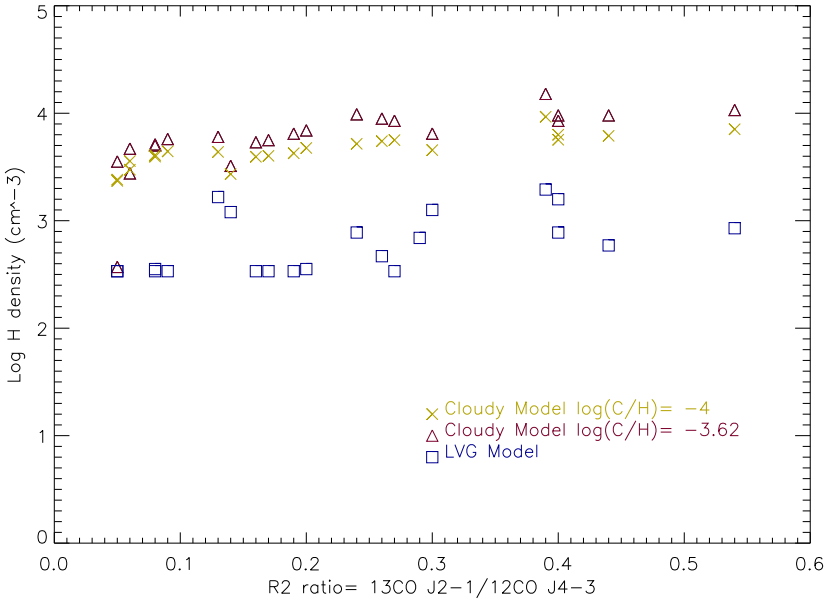

Figure 4.11 Cloudy Forced Temperature models are below the LVG predictions. Cloudy consistently predicts higher overall density but lower H_2 density than the LVG models.

The UV models made radically different predictions about the temperature and density of the cloud. Figures 4.12 and 4.13 plot the UV results next to the Forced Temperature ones. The UV models predict denser clouds $n_{\rm H} \approx 10^{5.5}$ that are all about 11 K.

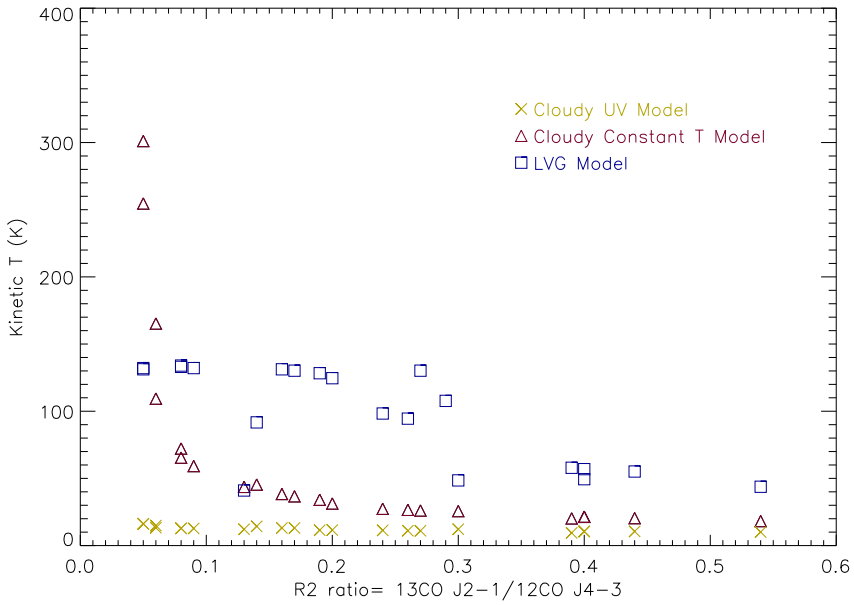

Figure 4.12 The UV models predict much cooler clouds with T $\approx 10.5K$. LVG predictions fall somewhere in between these predictions and those of Forced Temperature models. The label for Forced Temperature models is Constant T because the Cloudy command is `constant temperature`.

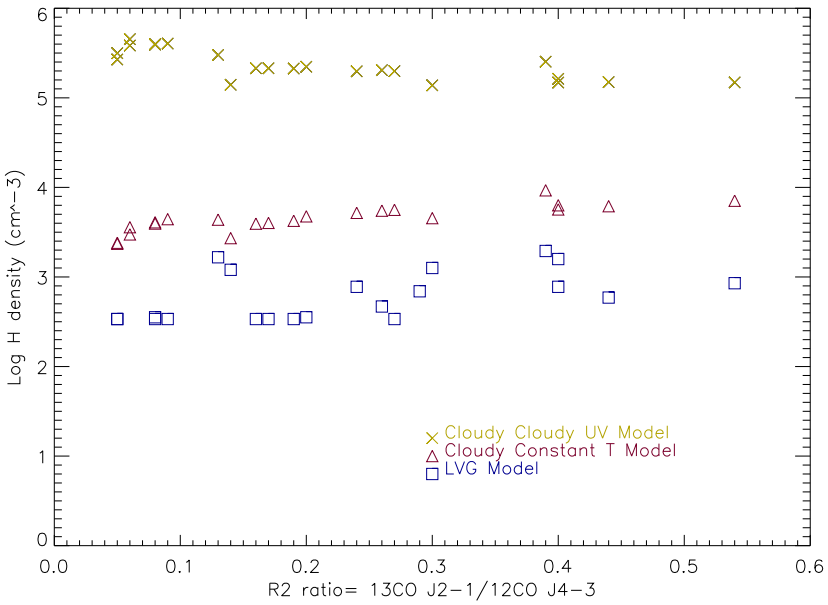

Figure 4.13 The UV models predict much denser clouds than either Forced temperature. Constant T = Forced temperature models because the Cloudy command is `constant temperature`.

4.3.5 Turbulent and Active Galactic Nucleus (AGN) Models

In case UV models are not appropriate for Clump 1 and or Clump 2, we ran models that were heated by turbulence and Active Galactic Nuclei (AGN). These models, surprisingly, produced

nothing new. Turbulent models were identical to Forced Temperature ones, probably because Cloudy treats the turbulent heating source as independent of gas physics. In Forced Temperature models, the cloud's heating was adjusted to make the gas a specific temperature. When turbulence was in place, it provided a physical means for that turbulence but did not change the cloud's spectrum. AGN,[2] on the other hand, altered the cloud's behavior to be identical to UV heating. Despite the fact that AGN spectra differ radically from UV spectra with high energy photons, both models created the same CO brightnesses.

4.4 Exclusion of CO $J = 7 \rightarrow 6$ in Cloudy

CO $J = 7 \rightarrow 6$ emission was initially excluded from the Cloudy runs because Cloudy failed to simultaneously match the observed CO $J = 4 \rightarrow 3$, CO $J = 7 \rightarrow 6$, [C I] $^3P_1 \rightarrow {}^3P_0$ and ^{13}CO $J = 2 \rightarrow 1$ intensities for any temperature and density. These four lines intensities were all divided by CO $J = 4 \rightarrow 3$, reducing the number of constraints to three:

- R1 = (CO $J = 7 \rightarrow 6$)/(CO $J = 4 \rightarrow 3$)
- R2 = (CO $J = 2 \rightarrow 1$)/(CO $J = 4 \rightarrow 3$)
- R3 = ([C I] $^3P_1 \rightarrow {}^3P_0$)/(CO $J = 4 \rightarrow 3$)

Only when CO $J = 7 \rightarrow 6$ was excluded could Cloudy match the other two ratios. When all three are put in as constraints, there was no good solution. We made various attempts to adjust metallicity (overall abundance of elements with atomic number greater than 2), dust abundance, ^{12}CO to ^{13}CO abundance, cosmic ray density, optical depth, different initial conditions, and the spectra of the incident photons but were unable to match all three ratios. In the future, as mentioned in Section 5.2, a cloud model should be able to match all three ratios.

[2]Active Galactic Nuclei are accretion disks around black holes. They can be bright in X-Rays and ultraviolet light, but the Milky Way's black hole is not terribly active in the present epoch.

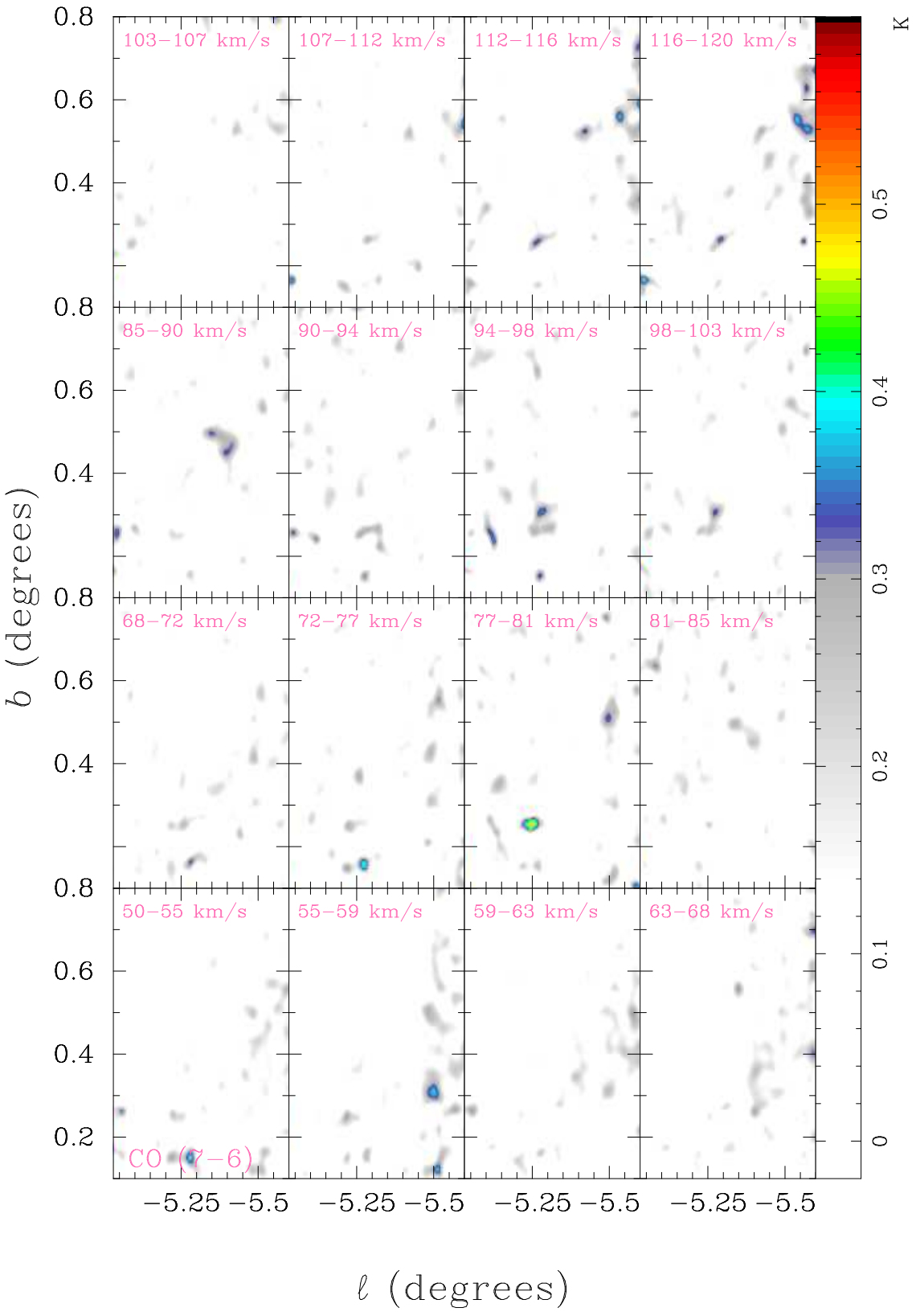

Figure 4.14 Clump 1 CO $J = 7 \rightarrow 6$ emission. These slices of the data cube show some very compact sources of CO $J = 7 \rightarrow 6$ not visible in Figure 1.6

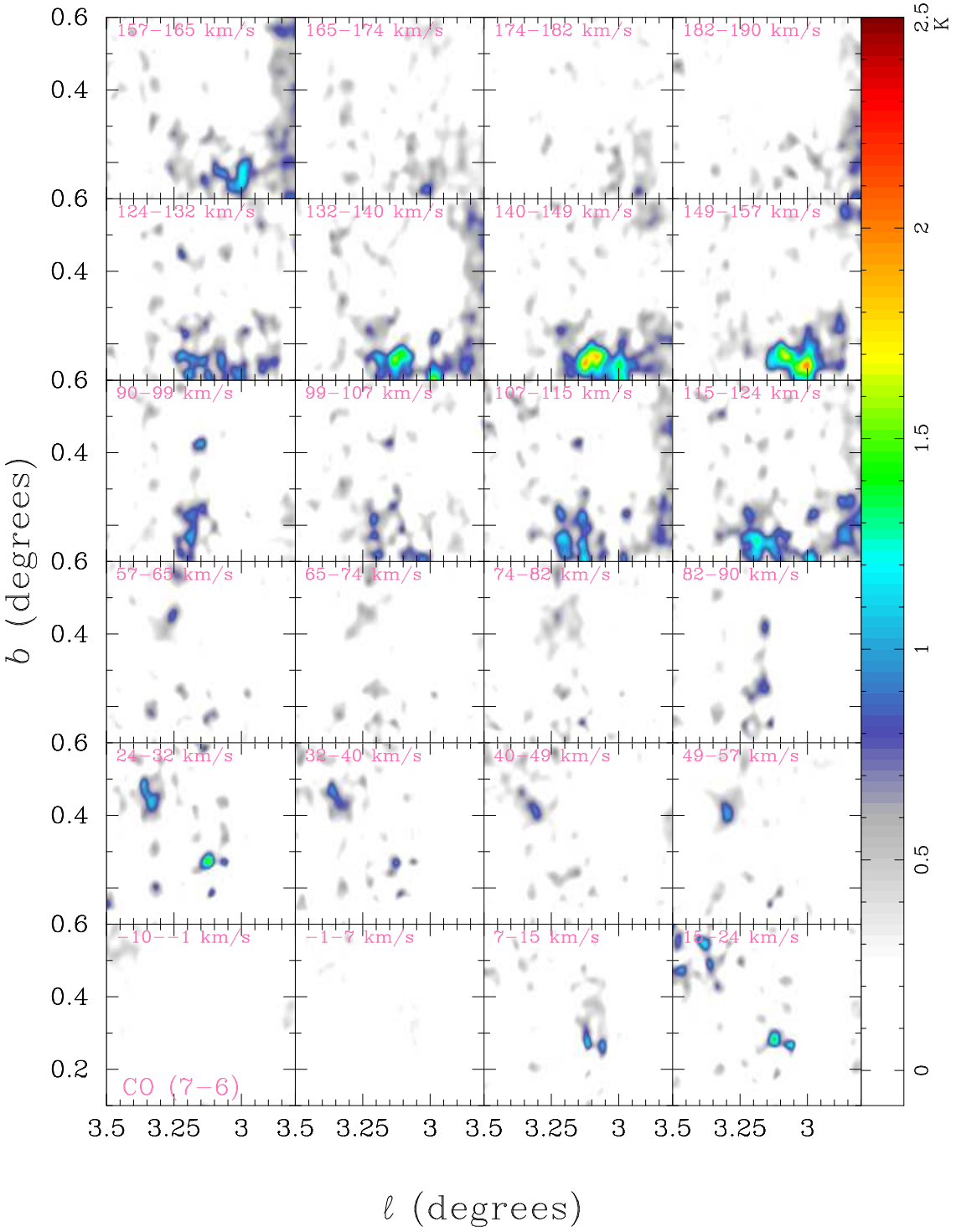

Figure 4.15 Clump 2 CO $J = 7 \rightarrow 6$ emission. As in Clump 1, the detailed velocity slices show some compact sources of CO $J = 7 \rightarrow 6$ emission. In addition, there is a significant sub-clump at $b = 0.1$ °, $\ell = 3.1$ °, v=145 km/s

4.5 Other Calculations of Physical Conditions

Oka et al. (1999) calculated the physical conditions in a cloud nearer to the GC than Clump 1 and Clump 2 using an LVG model. For the cloud CO 0.02-0.02 (ℓ = +0.02°, b = -0.02°), they used the CO $J = 1 \rightarrow 0$, CO $J = 3 \rightarrow 2$, and HCN J=1 $\rightarrow$ 0 lines to predict density and temperature. They found $n(\mathrm{H_2})= 10^{4.2}$ and $\mathrm{T}_{kinetic} = 60\mathrm{K}$.

Huettemeister et al. (1993) found a rotational temperature for a region very close to IGGC1 in Clump 1 based off ammonia transitions. They found $\mathrm{T}_{rot} = 20$ K which converts to $\mathrm{T}_{kinetic} \approx 20\mathrm{K}$.

4.5.1 Lower Limits

As suggested by CU-Boulder graduate student Adam Ginsberg, in the regions where CO $J = 7 \rightarrow 6$ is detected, the kinetic temperature should be above the excitation temperature of CO $J = 7 \rightarrow 6$. For more explanation of the temperatures, see § 2.1. For the CO $J = 7 \rightarrow 6$ transition at 371.5 μm, $\Delta E/k = 45K$, so we expect temperatures $\gtrsim 45$ in CO $J = 7 \rightarrow 6$ emitting regions.

Chapter 5

Conclusion and Future Directions

5.1 Conclusion

The Milky Way is home to two interesting gas clumps, Bania Clump 1 and 2. They reside roughly 1kpc from the GC and interact with the Galactic Bar in the Inner Galaxy (IG). Their unusual velocities and environment make the two clouds interesting targets to study, both kinetically and thermally.

We employed the velocity centroids technique to study the effects of turbulence in Clump 1 and 2. In our analysis, we show that Clump 2 is probably heated by turbulent dissipation. Clump 1, on the other hand, shows weaker evidence for turbulent dissipation. For this clump, stellar heating may be more significant and the nearby H II region G354.67+0.25 may be the culprit. The UV photons from this region may actually power a significant portion of Clump 1 with turbulence playing a small to negligible role.

The Cloudy spectral code was optimized to fit each Inner Galaxy Gas Clump (IGGC) within the macro clumps. Depending on the source of heating, Cloudy gives very different results: UV models are very dense and cold, while forced temperature models are warmer and less dense. Besides showing some ambiguities within itself Cloudy also disagree with results from an independent Large Velocity Gradient (LVG) model.

The velocity centroid analysis may help resolve some of the differences in the models. Clump 1 is probably better described by UV models since it shows weak evidence for turbulent heating. This would favor the models with T $\approx$ 10K and $n_{\rm H} \gtrsim 10^5$ cm^{-3}. Clump 2 is probably better fit by the turbulent models, which give $n_{\rm H} \approx 10^{3.5}$ and temperatures that scale strongly with the ^{13}CO $J = 2 \rightarrow 1$/ CO $J = 4 \rightarrow 3$ ratio.

5.2 Future Directions

The Herschel Space Observatory should be launched in late April 2009 and will begin exploring the infrared sky when it reaches position in a solar orbit. Once calibration is complete, we will begin seeing Clump 1 and 2 as never seen before. We can then start exploring some of the mysteries surrounding them. Of particular relevance to this paper will be what Herschel data has to say about the clumps' heating sources. In the following section, we hazard some predictions about what Herschel will see.

We can look for evidence of ultraviolet photons by looking at emission lines from N^+ and C^+. These two ions, with first ionization potentials of 14.5eV and 11.3eV, should exist only if there is some ultraviolet flux. If Clump 2 is heated only by turbulence, then Herschel should see no significant 158 μm, 205 μm, or 122 μm emission lines with its spectrometers, because these are C II and N II features. Clump 1, on the other hand, may show these emission lines because starlight could be an important source of heating. If the lines do show up, they should be close to the H II region G354.67+0.25. C II emission may extend farther into Clump 1 because its ionization

potential is below that of hydrogen, so it can exist outside of H II regions. N II should remain confined to the H II region because N^+ cannot exist where there are no ionizing photons.

If C II 158 μm emission is present in Clump 1, it can indicate whether the LVG or Cloudy model is more accurate. The C II cooling feature, with $\Delta E/k = 92K$ should be brighter than CO cooling if the gas is at or above 92K. This is because C II is a much more efficient coolant than CO (Dyson & Williams, 1997), so long as the temperature is high enough to excite it. A potential criticism with this argument is that the C II emission may come from a shell of gas surrounding each IGGC, whereas CO emission may come from within. This criticism is warranted, but there is a chance that these regions overlap. Comparison of Herschel's data cubes with those from the Antarctic Submillimeter Telescope and Radio Observatory (AST/RO) can reveal whether C II emission and CO emission are coincident or separate.

Regardless of expectations, Herschel's new view of the Inner Galaxy will be an exciting exploration into new territory. Never before have Clump 1 and Clump 2 been explored in high resolution with infrared detectors. The above predictions may be confirmed or refuted, but we eagerly await to see what Herschel finds. Most likely, Herschel's observations of the IG and beyond will reshape and rewrite our understanding of the interstellar medium.

Glossary

$M_\odot$ Solar Mass 1 $M_\odot$= 1.99 $\times 10^{30}$ kg

AGN Active Galactic Nucleus. This is an accretion disk around a supermassive black hole. They are present in very virulent forms (Quasars), but also in more quiescent forms as well in nearby galaxies.

AST/RO Antarctic Submillimeter Telescope and Radio Observatory

CO $J = 1 \rightarrow 0$ This notation refers to rotational states of Carbon Monoxide. The rotational energies of the states are quantized with energies E=B J (J+1) where B is a constant and J is a non-negative integer, J=0,1,2,3,... (Lequeux, 2005). Only transitions with ΔJ = $\pm$1 are allowed. The true energies of CO are slightly different from a rigid rotor, but the details are unnecessary for this text.

H II Emission from singly ionized hydrogen = H^+. "H II regions" are clouds where hydrogen is ionized. These are usually the active sites of star formation, where newly formed stars irradiate the gas from which they form.

H I Emission from Neutral (non-ionized) Hydrogen

HIGGS Herschel Inner Galaxy Gas Survey

HNCO Isocyanic acid

IDL Interactive Data Language

IG Inner Galaxy

IGGC Inner Galaxy Gas Clump

LVG Large Velocity Gradient

N II Emission from singly ionized nitrogen = N^+

pc 1 parsec (pc) is 3.26 light years or 3.09 $\times 10^{16}$ m.

PDF Probability Distribution Function: The normalized histogram of a function or array.

UV Ultra-Violet

Bibliography

Bally, J., Aguirre, J., Bradley, T. E., Cyganowsky, C., Dowell, D., Drosback, M., Neal J. Evans, Ginsburg, A., Glenn, J., Harvey, P., Nordhaus, M., Rosolowsky, E., Stringfellow, G. Walawender, J., & Williams, J. 2009, In Prep.

Bally, J., Stark, A. A., Wilson, R. W., & Henkel, C. 1987, ApJS, 65, 13

—. 1988, ApJ, 324, 223

Bania, T. M. 1977, ApJ, 216, 381

Bania, T. M., Stark, A. A., & Heiligman, G. M. 1986, ApJ, 307, 350

Carroll, B. W. & Ostlie, D. A. 2006, An introduction to modern astrophysics and cosmology (Institute for Mathematics and Its Applications)

Dahmen, G., Huettemeister, S., Wilson, T. L., Mauersberger, R., Linhart, A., Bronfman, L., Tieftrunk, A. R., Meyer, K., Wiedenhoever, W., Dame, T. M., Palmer, E. S., May, J., Aparici, J., & Mac-Auliffe, F. 1997, A&AS, 126, 197

Dyson, J. E. & Williams, D. A. 1997, The physics of the interstellar medium (The physics of the interstellar medium. Edition: 2nd ed. Publisher: Bristol: Institute of Physics Publishing, 1997. Edited by J. E. Dyson and D. A. Williams. Series: The graduate series in astronomy. ISBN: 0750303069)

ESA. 2009

Ferland, G. J. 2003, ARA&A, 41, 517

Frisch, U. 1995, Turbulence. The legacy of A.N. Kolmogorov (Cambridge: Cambridge University Press, —c1995)

Gustafsson, M., Brandenburg, A., Lemaire, J. L., & Field, D. 2006, A&A, 454, 815

Häfner, R., Evans, N. W., Dehnen, W., & Binney, J. 2000, MNRAS, 314, 433

Hepburn, K. L. H. 2008, The Milky Way Over Ontario, *http://antwrp.gsfc.nasa.gov/apod/ap080729.html*

Hily-Blant, P., Falgarone, E., & Pety, J. 2008, A&A, 481, 367

Huettemeister, S., Wilson, T. L., Bania, T. M., & Martin-Pintado, J. 1993, A&A, 280, 255

Law, C. J. 2007, PhD thesis, Northwestern University

Lazarian, A. 2008, Space Science Reviews, 176

Lequeux, J. 2005, The interstellar medium (The interstellar medium, Translation from the French language edition of: Le Milieu Interstellaire by James Lequeux, EDP Sciences, 2003 Edited by J. Lequeux. Astronomy and astrophysics library, Berlin: Springer, 2005)

Lis, D. C., Pety, J., Phillips, T. G., & Falgarone, E. 1996, ApJ, 463, 623

Martin, C. L., Harnet, J., Leppik, K., Tothill, N. F. H., & Stark, A. A. 2009

Oberst, T. E., Parshley, S. C., Stacey, G. J., Nikola, T., Löhr, A., Harnett, J. I., Tothill, N. F. H., Lane, A. P., Stark, A. A., & Tucker, C. E. 2006, ApJ, 652, L125

Oka, T., Geballe, T. R., Goto, M., Usuda, T., & McCall, B. J. 2005, ApJ, 632, 882

Oka, T., White, G. J., Hasegawa, T., Sato, F., & Miyazaki, A. 1999, ApJ, 515, 249

Pety, J. & Falgarone, E. 2003, A&A, 412, 417

Pilbratt, G. 2008, in COSPAR, Plenary Meeting, Vol. 37, 37th COSPAR Scientific Assembly, 2437–+

Sawada, T., Hasegawa, T., Handa, T., & Cohen, R. J. 2004, MNRAS, 349, 1167

Shore, S. N., Larosa, T. N., Chastain, R. J., & Magnani, L. 2006, A&A, 457, 197

Stark, A. A. & Bania, T. M. 1986, ApJ, 306, L17

Stark, A. A., Martin, C. L., Walsh, W. M., Xiao, K., Lane, A. P., & Walker, C. K. 2004, ApJ, 614, L41

van der Tak, F. F. S., Belloche, A., Schilke, P., Güsten, R., Philipp, S., Comito, C., Bergman, P., & Nyman, L.-Å. 2006, A&A, 454, L99

Williams, J. P., de Geus, E. J., & Blitz, L. 1994, ApJ, 428, 693

Wolfire, M. G., Hollenbach, D., McKee, C. F., Tielens, A. G. G. M., & Bakes, E. L. O. 1995, ApJ, 443, 152